OXFORD

Human Molecular Genetics, 2016, Vol. 25, No. 17 3654–3675

doi: 10.1093/hmg/ddw212
Advance Access Publication Date: 4 July 2016
Original Article

ORIGINAL ARTICLE

An enhanced Q175 knock-in mouse model of Huntington disease with higher mutant huntingtin levels and accelerated disease phenotypes

Amber L. Southwell[1,*], Amy Smith-Dijak[2], Chris Kay[1], Marja Sepers[2], Erika B. Villanueva[1], Matthew P. Parsons[2], Yuanyun Xie[1], Lisa Anderson[1], Boguslaw Felczak[1], Sabine Waltl[1], Seunghyun Ko[1], Daphne Cheung[1], Louisa Dal Cengio[1], Ramy Slama[1], Eugenia Petoukhov[1], Lynn A. Raymond[2] and Michael R. Hayden[1,*]

[1]Centre for Molecular Medicine and Therapeutics, Child and Family Research Institute and [2]Department of Psychiatry, Djavad Mowafaghian Centre for Brain Health, University of British Columbia, Vancouver, British Columbia, Canada

*To whom correspondence should be addressed at: Tel: +604-875-3535; Fax: +604-875-3819; Email: asouthwell@cmmt.ubc.ca(A.L.S.); mrh@cmmt.ubc.ca(M.R.H)

Abstract

Huntington disease (HD) model mice with heterozygous knock-in (KI) of an expanded CAG tract in exon 1 of the mouse huntingtin (Htt) gene homolog genetically recapitulate the mutation that causes HD, and might be favoured for preclinical studies. However, historically these mice have failed to phenotypically recapitulate the human disease. Thus, homozygous KI mice, which lack wildtype Htt, and are much less relevant to human HD, have been used. The zQ175 model was the first KI mouse to exhibit significant HD-like phenotypes when heterozygous. In an effort to exacerbate HD-like phenotypes and enhance preclinical utility, we have backcrossed zQ175 mice to FVB/N, a strain highly susceptible to neurodegeneration. These Q175F mice display significant HD-like phenotypes along with sudden early death from fatal seizures. The zQ175 KI allele retains a floxed neomycin resistance cassette upstream of the Htt gene locus and produces dramatically reduced mutant Htt as compared to the endogenous wildtype Htt allele. By intercrossing with mice expressing cre in germ line cells, we have excised the neo cassette from Q175F mice generating a new line, Q175FΔneo (Q175FDN). Removal of the neo cassette resulted in a ∼2 fold increase in mutant Htt and rescue of fatal seizures, indicating that the early death phenotype of Q175F mice is caused by Htt deficiency rather than by mutant Htt. Additionally, Q175FDN mice exhibit earlier onset and a greater variety and severity of HD-like phenotypes than Q175F mice or any previously reported KI HD mouse model, making them valuable for preclinical studies.

Introduction

Huntington disease (HD) in an inherited, fatal neurodegenerative disease affecting approximately 1:10,000 individuals of European descent (1,2). HD is characterized by selective loss of striatal medium spiny neurons, forebrain atrophy, progressive motor and cognitive decline and psychiatric disturbance (3).

Received: April 1, 2016. **Revised:** June 7, 2016. **Accepted:** June 28, 2016

While moderately effective symptomatic treatments are available for HD, including antipsychotics and antidepressants for psychiatric symptoms and Tetrabenazine for chorea, there are currently no disease modifying therapies (4). Considering that HD typically has a disease course lasting 15–20 years, and that patients require full nursing home care for a substantial portion of that interval (3), HD presents a significant societal burden and unmet medical need. Thus, there is a need for faithful mouse models of HD for use in preclinical studies of disease mechanisms, therapeutic target validation and experimental therapeutic development.

HD is caused by expansion of a polyglutamine (polyQ)-encoding tract in exon 1 of the huntingtin (*HTT*) gene to greater than 35 CAG repeats (5). True genetic models of HD, in which the 7 CAG repeats of endogenous mouse huntingtin (*Hdh*) are expanded to lengths that result in adult onset HD (36–60 CAG) (6) does not result in overt HD-like phenotypes in mice (7), possibly due to the short life span or of mice. Thus, strategies have been employed to increase the toxicity of muHtt in mice in order to model HD. These include the use of CAG tract lengths well above those required to cause juvenile onset HD (71–250 CAG), either knocked in to the endogenous mouse Htt gene (8–12) or within a human transgene of either the full-length human HTT cDNA (13) or gene (14–16) or a more toxic N-terminal fragment of human HTT (17,18). This has resulted in a large variety of mouse models of HD, none of which fully recapitulate the human disease (19,20), complicating the selection of appropriate models for preclinical studies.

Heterozygous knock-in (KI) mice most closely recapitulate the genetic mutation that causes HD, and for that reason might be favoured for preclinical testing. However, historically these models have failed to sufficiently phenotypically recapitulate the human disease (7,11). To increase the severity of phenotypes to a useful level, homozygous KI mice, which entirely lack wild-type huntingtin (wtHtt) and are, therefore, much less relevant to human HD, have been studied. The C57BL/6JQ175KI model (zQ175), which arose as a spontaneous expansion of the CAG140 KI line (8,21), is of particular interest because it is the first KI mouse to exhibit significant HD-like phenotypes as a heterozygote (21,22). FVB mice are generally more susceptible to neurodegeneration than C57BL/6 mice, and YAC128 HD model mice on the FVB background have earlier onset and increased severity of phenotypes as compared to YAC128 mice on the C57BL/6 background (23). Additionally, a recent report of BACHD mice on the C57BL/6 background found behavioural abnormalities, but no evidence of striatal degeneration (24). This is in contrast to multiple previous reports describing significant striatal degeneration in BACHD mice on the FVB/N background (14,25, 26). In an effort to reduce pre-clinical testing duration and increase phenotypic severity, we have backcrossed zQ175 mice ten generations to FVB/N (Q175F). Basic characterization was then begun using endpoints previously validated in the zQ175 line. Sudden early death from fatal seizures was observed in Q175F heterozygous and homozygous mice confounding full characterization. Because this is not consistent with HD, we postulated that the previously reported natural susceptibility to seizures of FVB/N mice (27) was somehow exacerbated in Q175F mice.

The zQ175 and Q175F mice have a floxed neomycin (neo) resistance gene embedded upstream of the targeted *Htt* gene locus (8), and this neo cassette is known to interfere with gene expression (28,29), suggesting that Q175F mice were hypomorphic at the mutant Htt (muHtt) locus. Using mice that express the cre recombinase in germ line cells (30), we excised the neo cassette, generating a new line, Q175FΔneo (Q175FDN). We then performed rigorous side by side phenotypic assessment of littermate wild-type (WT), heterozygous (HET), and homozygous (HOM) Q175F and Q175FDN mice, including brain Htt levels, longevity, longitudinal body weight, accelerating rotarod, spontaneous climbing, and forelimb grip strength, open field exploration, object learning, forced swimming, testis weight, neuropathology and brain histology. Additional characterization was then performed in Q175FDN mice only, including swimming T-maze, Striatal expression of HD-related genes, and electrophysiological characterization of striatal projection neurons (SPNs). Neo excision resulted in a ~2 fold increase in mutant Htt protein in the brain of Q175FDN mice. Phenotypic severity in mouse models of HD is tightly linked to muHtt levels (31). Consistent with this, we found that Q175FDN mice exhibited earlier onset and a greater variety and severity of HD-like phenotypes as compared to Q175F mice. Our characterization of Q175FDN mice suggests this model offers an improved reproduction of HD phenotypes with the mutation in the knocked-in heterozygous state, of high value for preclinical studies.

Results

zQ175 mice on the FVB background (Q175F) die from fatal seizures

Backcrossing to the FVB/N background strain resulted in sudden death from ~3 mo of age in both HET and HOM Q175F mice. These mice appeared generally healthy one day and were found dead the following day. Necropsy revealed internal organs to be normal (data not shown). Analysis of 24 h infrared video revealed that mice had generalized tonic-clonic seizures immediately prior to death, indicating that death occurred by sudden, fatal seizures. PCR analysis of CAG tract length revealed that some drift of approximately 30 base pairs occurred during 10 generation backcrossing, resulting in slightly higher CAG tract length in Q175F than in zQ175 mice (Supplementary Material, Fig. S1).

Excision of the neo cassette from the Q175 knock-in transgene restores muHtt levels

CAG140 KI mice, the precursor line to zQ175 mice, exhibit reduced muHtt expression (32) that may result from the neomycin selection cassette (pgk-neo) embedded upstream of the *Htt* gene. Thus, zQ175 and Q175F mice would also be expected to have reduced muHtt expression. We crossed Q175F mice to Vasa-cre mice, which express cre in germ line cells (30) to excise the neo cassette and generate a new line, Q175FΔneo (Q175FDN). To verify excision, primers were designed to amplify a 286bp region around the original HindIII insertion site (AGCTT) of the pgk-neo cassette, approximately 1.3kb upstream of the transcription start site (8). This resulted in the expected product from WT mice, and a larger product from Q175FDN mice. Sequencing of these products revealed the expected reference sequence in WT mice, and a residual 54bp sequence containing one LoxP site in Q175FDN mice (Figure 1A) . The margin of mouse *Hdh* exon 1 and human *HTT* exon 1 was verified to be 28bp downstream of the initiating *Hdh* start codon in chimeric exon 1 of Q175F and Q175FDN. More than 200 CAG repeats were observed within this chimeric exon 1, although repeat number varied between animals and could not be precisely determined by direct sequencing of exon 1 PCR products. PCR analysis of CAG tract length in Q175F and Q175FDN lines revealed some variation in tract length indicative of expected repeat instability.

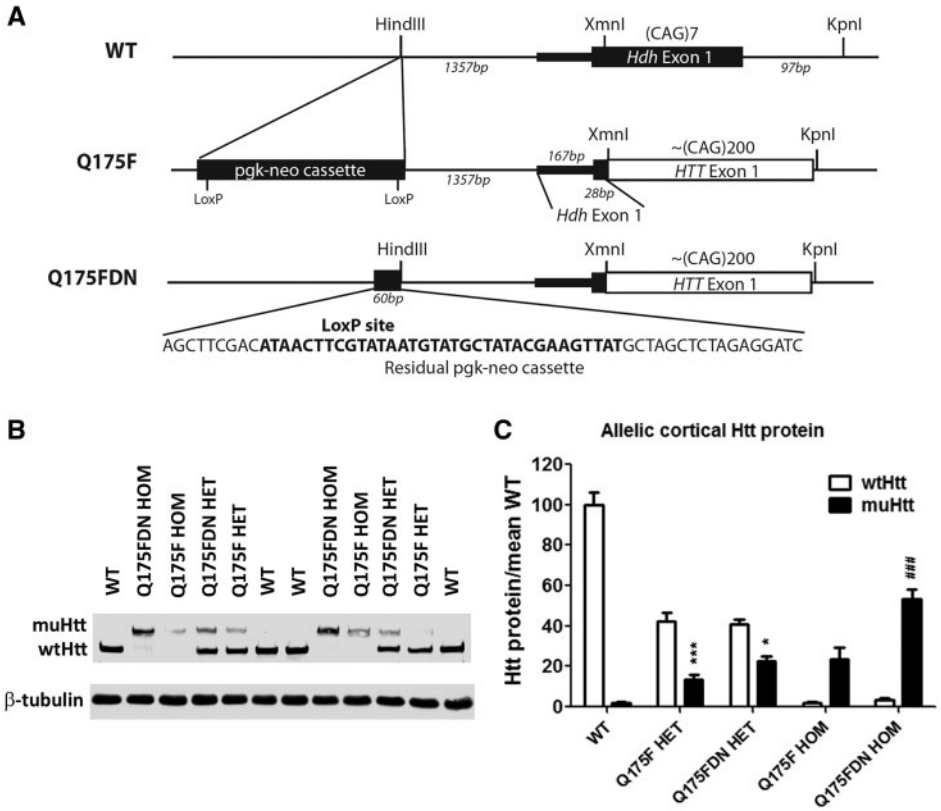

Figure 1. Deletion of the neo cassette in the Q175 knock-in allele restores muHtt levels. (**A**) Schematic of the Q175F knock-in locus and recombination between LoxP sites to remove the neomycin selection cassette with phosphoglycerol kinase promoter (pgk-neo). The pgk-neo cassette was originally inserted at an endogenous *Hind*III restriction site located 1.3kb upstream of *Hdh* exon 1 (chr5:34760378-34760383, GRCm38). In Q175FDN mice, a residual 60bp pgk-neo sequence containing a single LoxP site remains at the endogenous *Hind*III cut site after cre recombination (shown sequence is between chr5:34760382-34760383). A *Hind*III recognition sequence remains intact at the 5' end of the residual sequence. Chimeric exon 1 in Q175F retains the initial 28bp of *Hdh* exon 1 coding sequence, followed by fully human*HTT* exon 1 sequence until a *Kpn*I restriction site within *Hdh* intron 1. The first 97bp of *Hdh* intron 1 are missing in the Q175 KI allele, corresponding to the *Kpn*I cut site used to insert the *HTT* exon 1 sequence (chr5:34762202-34762207). (**B**) Allelic separation immunoblot showing levels of full-length endogenous wtHtt protein and Q175 knock in muHtt protein in WT, HET, and HOM mice from the Q175F and Q175FDN lines. (**C**) Quantitation of both alleles of Htt protein in an n of 4 animals per genotype. *=different from wt allele in same genotype. #=different from same genotype of Q175F line. *= $P < 0.05$, ***= $P < 0.001$.

However, the tract lengths and variability were similar in the two lines (Supplementary Material, Fig. S2)

Cortical and striatal Htt protein was evaluated in WT, HET, and HOM Q175F and Q175FDN brains using allelic separation immunoblotting(Figure 1B,C) . HTT levels in the cortex and striatum were found to be similar, so data are only shown for cortex. Q175F mice were found to be hypomorphic at the Q175 knock-in allele with the mean muHtt protein level in HET cortices being ~32% of the mean endogenous wtHtt level (one copy) in the same genotype. In Q175FDN mice, this is increased to ~55%, though this increase did not reach significance by *post hoc* analysis. In homozygous Q175F mice, the mean total Htt level is ~24% of the mean total Htt level in WT mice. In Q175F HOM mice, this is significantly increased to ~53% ($P < 0.001$). Thus excision of the neo cassette in the Q175 knock-in transgene results in a roughly two-fold increase in muHtt protein level in the brain.

Restoring muHtt in Q175FDN mice prevents fatal seizures but reduces survival due to HD-like deterioration

After deletion of the neo cassette, Q175FDN mice were no longer susceptible to fatal seizures. However, these mice did display a decline in general health and clinical signs consistent with HD, including ataxia, weight loss, and postural changes from ~8 mo in HOM mice and ~12 mo in HET mice. After the onset of clinical signs, mice were monitored daily for signs that they had reached a humane endpoint, after which they were euthanized. Survival deficits were noted for Q175FDN HOM mice from 9 mo of age and HET mice from 13 mo of age (Figure 2A), indicating a period of overt clinical decline lasting at least 1 month.

Restoring muHtt in Q175FDN mice accelerates peripheral pathology

Body weight

Progressive body weight loss if a feature of HD (33). While N-terminal fragment HD mouse models share this feature, mouse models expressing full-length human HTT display increased body weight (34,35). Thus, body weight was evaluated every 2 months from 2 to 12 months of age. Trends for reduced body weight compared to WT littermates were observed for Q175F HOM males and Q175F HET females (Figure 2B and C). While there was a significant effect of genotype by two-way ANOVA ($P < 0.0001$ males, $P = 0.008$ females) for this measure, data at individual time points failed to reach significance by *post hoc* analysis. Conversely, Q175FDN mice displayed significantly reduced body weight compared to WT

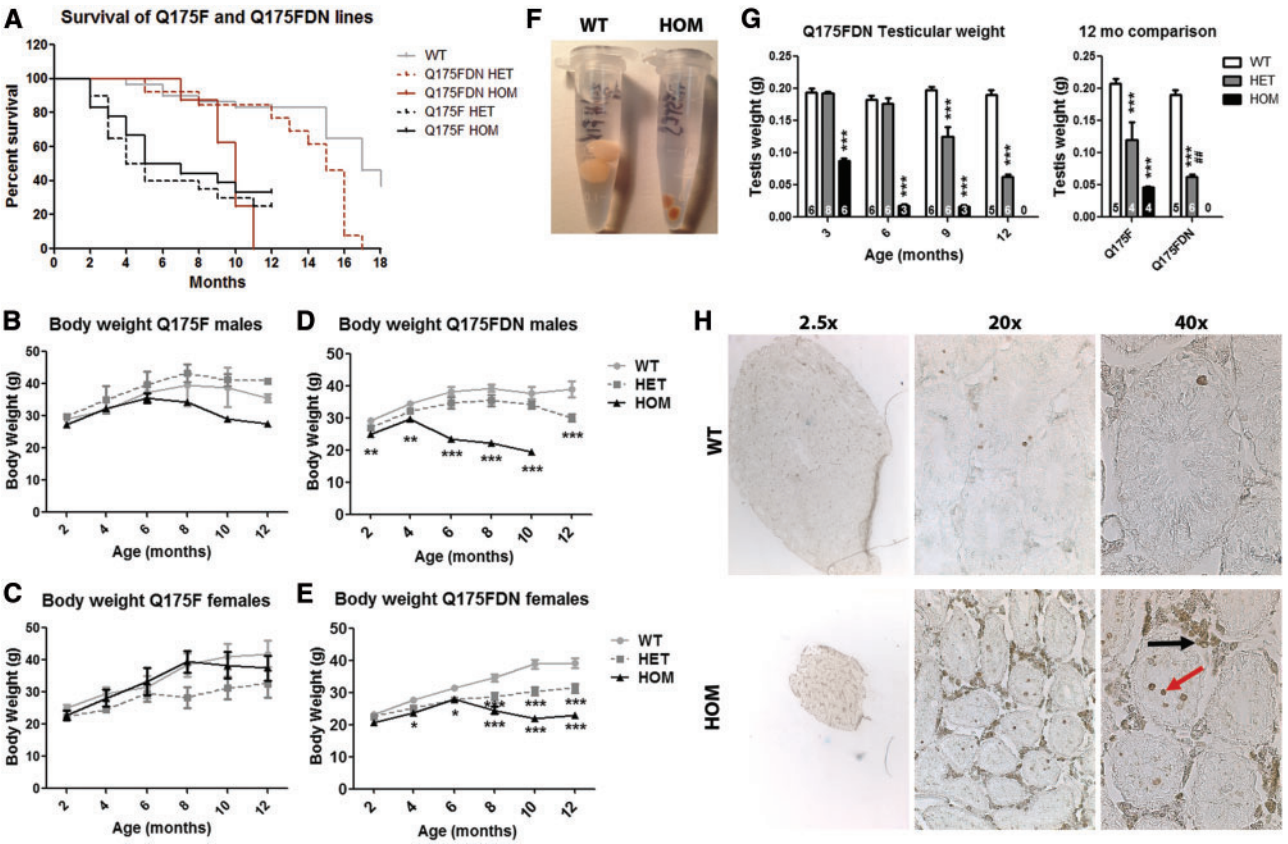

Figure 2. Survival and peripheral pathology. (**A**) Survival was compared for WT, HET, and HOM mice of Q175F and Q175FDN lines. The Q175F line was followed for 12 months. Both HET and HOM mice display dramatically reduced survival from approximately 3 months of age. The Q175FDN line was followed for 18 months. HOM mice display reduced survival from 9 months of age, and HET mice from 13 months of age. (**B–E**) body weight of (B,D) male and (C,E) female mice was assessed at 2 month intervals from 2 to 12 months of age in WT, HET, and HOM (B,C) Q175F and (D,E) Q175FDN mice. Weight loss was observed in transgenics of both lines, however, this was earlier and more severe in Q175FDN mice than in Q175 mice. (**F**) Photograph of 9-month old Q175FDN WT and HOM post-perfusion testes. (**G**) Testicular weight was assessed in Q175FDN mice at 3, 6, 9 and 12 months of age (left graph) and Q175F mice at 12 months of age (right graph). Q175FDN HOM mice display significant loss of testis weight from 3 months of age, the earliest time point evaluated. By 6 months of age, testis weight loss is over 90% in this genotype. Q175FDN HET mice display reduced testis weight from 9 months of age that is more pronounced at 12 months of age. Q175F HET and HOM mice also display reduced testis weight at 12 months of age, though it is not as severe as in the Q175FDN line. (**H**) TUNEL staining in 9 month old Q175FDN WT and HOM testes showing reduced size of seminipherous tubules with apoptotic degeneration of spermatogenic cells (red arrow), and the surrounding Leydig cells (black arrow). *=different from WT same age/line. #=different from same genotype of Q175F line. *= $P < 0.05$, **= $P < 0.01$, ***= $P < 0.001$.

littermates from 2 to 12 months of age for male HOM and HET mice, respectively, and from 4 and 6 months of age for female HOM and HET mice, respectively (Figure 2D and E). Thus, the body weight loss phenotype was accelerated/exacerbated in Q175FDN mice with higher muHtt levels.

Testicular degeneration

Testis degenerate in HD mice and men (36–38). Therefore, testicular degeneration was evaluated by weight of post-perfusion testis. Q175FDN testis were collected at 3, 6, 9 and 12 months of age, while Q175F testis were only collected at 12 months of age (WT mice and the 30–40% surviving HET and HOM mice), the only perfusion time point studied for this line. Q175FDN testis were found to be dramatically atrophied from 3 months of age for HOM mice (the earliest time point evaluated), weighing approximately 45% of WT testis. By 6 months of age, the testis of Q175FDN HOM males weighed less than 10% of their WT littermates. This was again observed at 9 months of age (Figure 2F and G left panel). No Q175FDN HOM males survived to 12 months of age, so this measure could not be evaluated at this time point in this genotype. In Q175FDN HET mice, testis appeared normal at 3 and 6 months of age, but showed progressive atrophy from 9 months of age (mean 63% of WT testis weight) with increasing severity at 12 months of age (mean 33% of WT testis weight) (Figure 2G, left panel). Q175F males at 12 months of age displayed significant testicular atrophy for both HET and HOM mice (mean 58% and 22% of WT testis weight, respectively). However, the mean testis weight of Q175FDN HETs was significantly less than for Q175F HETs (Figure 2G, right panel), indicating worsening of progressive testicular degeneration as a result of the higher levels of muHtt in Q175FDN mice. Terminal deoxynucleotidyl transferase dUTP nick end labeling (TUNEL) staining in 9 month old Q175FDN HOM testis revealed smaller seminiferous tubules with apoptotic spermatogenic cells as well as dramatic apoptotic degeneration of the surrounding Leydig cells (Figure 2H).

Restoring muHtt in Q175FDN mice accelerates HD-like behavioural changes

Motor behaviour

Chorea and motor deficits are cardinal features of HD (33), and clinical onset of HD is defined by onset of motor symptoms (39).

Motor performance was assessed by longitudinal accelerating rotarod and spontaneous climbing assays conducted every 2 months from 2 to 12 months of age and by longitudinal forelimb grip strength testing every 3 months from 3 to 9 months of age. Q175F and Q175FDN mice performed normally during fixed speed rotarod training and accelerating rotarod testing at 2 months of age, indicating the absence of motor deficits or motor learning deficits at this time point (Figure 3A and B). HET and HOM mice of both lines underwent a progressive decline in rotarod performance that was significantly different from WT littermates by 4 and 6 months of age in Q175F and Q175FDN HOM mice, respectively, and from 8 months of age in Q175FDN HET mice (Figure 3C and D). Despite an obvious decline in performance in Q175F HET mice, differences from WT mice did not reach statistical significance due to the higher inter-animal variability that was observed in this line as compared to the Q175FDN line. Additionally Q175FDN HOM mice were more impaired than Q175F HOM mice after onset of overt clinical signs, approximately 8 months of age (Figure 3C and D). Spontaneous climbing behaviour was normal in both lines of mice at 2 months of age, again indicating that this time point is pre-onset for motor phenotypes. HOM mice of both lines exhibited increased latency to begin climbing and decreased time spent climbing from 8 months of age. HET mice of both lines exhibited declining spontaneous climbing from approximately 8 months of age, but similar to rotarod performance, this did not reach significance for the Q175F line and was only statistically different from WT climbing performance in Q175FDN HET mice (Figure 3 E–H). Q175F HOM mice exhibited normal forelimb grip strength at 3 months of age, and reduced forelimb grip strength at 6 months of age. At 9 months of age, inter-animal variability was very high, resulting in no significant difference from WT littermates. Q175F HET forelimb grip strength was normal at all assessed time points (Figure 3I). Q175FDN HET and HOM mice also had normal forelimb grip strength at 3 months of age. Q175FDN HOM grip strength was significantly reduced from 6 months of age, and Q175FDN mice also exhibited impaired forelimb grip strength at 9 months of age (Figure 3J). The greater magnitude change from WT littermates observed in Q175FDN HOMs compared to Q175F HOMs and the observable phenotype in Q175FDN HET mice indicate that the greater muHtt expression in this line results in exacerbated muscle weakness.

Anxiety-like behaviour

Anxiety is a common feature of prodromal and manifest HD (33). Anxiety-like behaviour was assessed by time spent in the centre during the exploration of a brightly lit open field at 3, 6, and 9 months of age in Q175FDN mice and at 6 months of age in Q175F mice. Exploratory activity, as measured by total distance travelled, was normal in Q175FDN HET mice, Q175FDN HOM mice at 3 and 6 months of age, and in Q175F HET and HOM mice at 6 months of age. Hypoactivity during open field exploration was observed in Q175FDN HOM mice at 9 months of age (Figure 4A). Q175FDN mice displayed a progressive anxiety-like phenotype. At 3 months of age, both HET and HOM mice spent a similar amount of time in the centre of the field as WT littermates. At 6 months of age, HOM mice spent a reduced amount of time in the centre of the field, indicating anxiety. At 9 months of age, both HET and HOM mice displayed this anxiety-like behaviour (Figure 4B, left panel). Q175F mice were only assessed for this measure at 6 months of age, a time point at which both HET and HOM mice spent a similar amount of time in the centre of the field as WT littermates, indicating the absence of anxiety-like behaviour at this time point (Figure 4B, right panel). The anxiety phenotype apparent in Q175FDN HOM mice at this time point indicates that the higher muHtt levels exacerbate anxiety-like behaviour in the neo deleted line.

Depressive-like behaviour

Depression is the most common psychiatric symptom of HD (33), and its recapitulation in mouse models (40) indicates that it is truly a feature of the disease and not the result of stresses related to living in an HD family. Depressive-like behaviour was assessed by immobility during forced swimming at 3, 6, 9 and 12 months of age in Q175FDN mice and at 12 months of age in Q175F mice. Q175FDN mice displayed a progressive depressive-like phenotype with HOM mice spending significantly more time immobile than WT littermates as early as 3 months of age with the magnitude of change increasing greatly from 6 months of age. Q175FDN HET mice performed normally during this test at 3 months of age, but displayed depressive-like behaviour from 6 months of age with the magnitude of change increasing at 12 months of age (Figure 4C, left panel). Conversely, Q175F HET and HOM mice performed similar to WT littermates on this test at 12 months of age, the only time point assessed (Figure 4C, right panel). The absence of this phenotype in the Q175F line combined with the early and severe phenotype in the Q175FDN line indicates that depressive-like behaviour is tightly linked to muHtt level.

Cognitive behaviour

Cognitive decline is a feature of HD, though the extent can vary greatly (33). Most commonly, higher level thinking, such as executive function, is most affected (41). Cognitive changes can precede onset of motor symptoms in prodromal HD (33) and in HD mouse models (42). Cognitive performance was evaluated by object location learning and recognition assays (Figure 5A and B) at 3, 6 and 9 months of age in Q175FDN mice and at 6 months of age in Q175F mice. Though inter-trial differences failed to reach *post hoc* significance, there was a significant effect of trial by two-way ANOVA for preference for a known object in a novel location (Figure 5C, $P = 0.0006$) and preference for a novel object (Figure 5D, $P = 0.0005$) and no effect of genotype in either assay, suggesting that spatial learning and object recognition occurs similarly in all three genotypes at 6 months of age. Conversely, Q175FDN mice displayed progressive impairment in both learning assays. Q175FDN HOM mice failed to show a preference for a known object in a novel location or a novel object as early as 3 months of age, the earliest time point evaluated (Figure 5E and F). Q175FDN HET mice, however, performed normally on both assays at 3 months of age. At 6 months of age, Q175FDN HET mice did show a preference for a known object in a novel location, indicating that spatial learning is still intact (Figure 5G). They did not, however, show a preference for a novel object, indicating impaired object recognition (Figure 5H). As Q175F mice performed normally in both assays at this age, this indicates an exacerbation of cognitive decline by higher muHtt levels. At 9 months of age, Q175FDN HET mice displayed impairment in both object learning assays (Figure 5I and J), indicating impaired spatial learning and object recognition.

Additional cognitive assessment was performed only in Q175FDN mice by swimming T-maze acquisition and reversal learning at 3, 6, 9 and 12 months of age. Supporting the object learning data, progressive cognitive decline was observed. At 3 months of age, acquisition learning was normal in Q175FDN HOM mice (Figure 6A). However, reversal learning was impaired

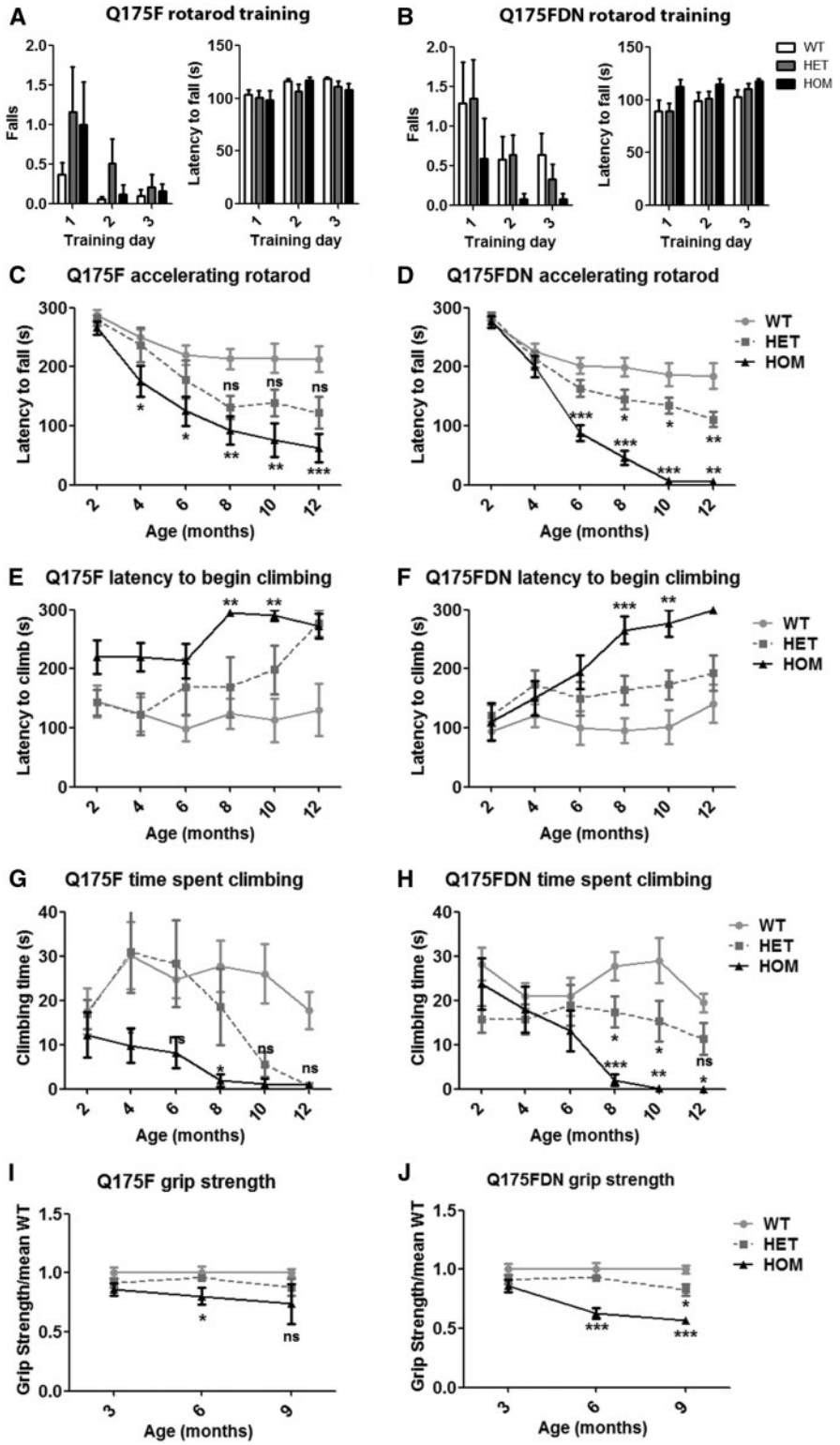

Figure 3. Q175F and Q175FDN mice display progressive motor deficits. (**A,B**) No genotypic effects were observed on motor learning during rotarod training at 2 months of age in either line. (**C,D**) The accelerating rotarod was used at 2 month intervals from 2 to 12 months of age to assess longitudinal motor performance. Q175F HOM and Q175FDN HET and HOM mice display significantly decreased latency to fall from the rotarod. While there was a substantial trend toward reduced latency to fall in Q175F HET mice, this did not reach significance by post hoc analysis. (**E–H**) Spontaneous climbing behaviour was assessed at 2 month intervals from 2-12 months of age. (E,F) HOM mice of both lines display significantly increased latency to begin climbing from 8 months of age. (**G,H**) HOM mice of both lines and HET Q175FDN mice display decreased total time spent climbing from 8 months of age. A trend toward reduced time spent climbing was observed in Q175F mice, but this did not reach post hoc significance. (**I,J**) Grip strength was assessed at 3, 6 and 9 months of age. (I) Q175F HOM mice display reduced grip strength at 6 months of age. (J) At 6 months of age Q175FDN HOM mice display reduced grip strength, and at 9 months of age both HET and HOM mice display reduced grip strength. *=different from WT same age/line, ns = not significant, *= $P < 0.05$, **= $P < 0.01$, ***= $P < 0.001$.

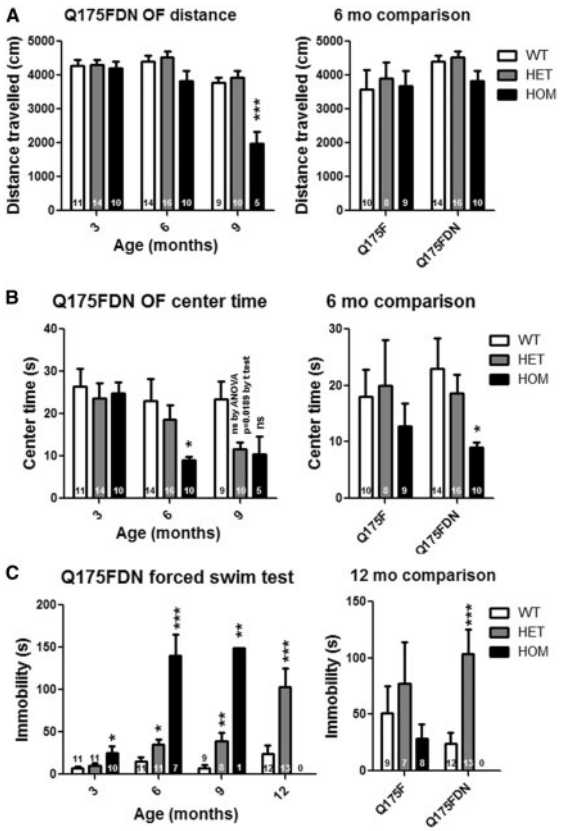

Figure 4. Q175FDN mice display anxiety and depressive-like behaviour. (**A**) Exploratory activity was assessed by total distance travelled during a 10-min exploration of a brightly lit open field at 3, 6 and 9 months of age in Q175FDN mice and at 6 months of age in Q175F mice. No genotypic effects were observed at 3 or 6 months of age. However, Q175FDN HOM mice were hypoactive at 9 months of age. (**B**) anxiety-like behaviour was assessed by time spent in the centre of the open field. As compared to WT littermates, Q175FDN HOM mice display anxiety-like behaviour from 6 months of age and HET mice from 9 months of age. Conversely, no genotypic effects were seen in Q175F mice at 6 months of age. (**D**) Depressive like behaviour was assessed by immobility during forced swimming in at 3, 6, 9 and 12 months of age in Q175FDN mice and at 12 months of age in Q175F mice. Q175FDN HOM mice display depressive-like behaviour from 3 months of age that increased in severity by 6 months of age. Q175FDN HET mice display depressive-like behaviour from 6 months of age that increased in severity by 12 months of age. Conversely, no significant effects of genotype were observed in Q175F mice at 12 months of age. *=different from WT same age/line, ns = not significant, *= $P < 0.05$, **= $P < 0.01$, ***= $P < 0.001$.

at this early time point (Figure 6B). At 6 months of age HOM mice also displayed impaired acquisition learning (Figure 6C) despite no change in swimming speed compared to WT littermates (data not shown). By 9 months of age, swimming speed was greatly impaired in HOM mice, so learning assessment was not performed. Q175FDN HET mice displayed normal swimming T-maze acquisition and reversal learning at 3 and 6 months of age (Figure 6A–D). At 9 months of age acquisition was normal, but reversal learning was impaired (Figure 6E and F), and by 12 months of age, both types of learning were impaired in Q175FDN HET mice (Figure 6G and H).

Restoring muHtt in Q175FDN mice accelerates HD-like neuropathology

HD-like neuropathology, which includes selective forebrain atrophy and loss of white matter (43,44), and brain histology was evaluated at 3, 6, 9 and 12 months of age in Q175FDN mice and at 12 months of age in Q175F mice.

Regional brain weight

Whole brain weight was found to be significantly reduced in Q175FDN HOM mice by 8.8% at 3 months of age, the earliest time point evaluated, and by 19.4% from 12 months of age in Q175FDN HET mice (Figure 7A, left panel). At 12 months of age, Q175F HOM mice displayed similar reductions in whole brain weight (mean 21%) as the one Q175FDN HOM mouse that survived to this time point (19.4%). However, Q175F HET mice failed to display whole brain atrophy at this time point, and Q175FDN HET brains were significantly smaller than Q175F HET brains (Figure 7A right panel). When only forebrain weight was considered, Q175FDN HOM mice, again showed significant atrophy of 10% at the earliest time point evaluated, 3 months of age, progressing to 20.4% by 12 months of age. Q175FDN HET mice showed significant atrophy of 4.4% by 6 months of age progressing to 6.8% at 12 months of age (Figure 7B, left panel). Similar to whole brain weight, at 12 months of age, Q175F HOM mice showed demonstrable atrophy of 23.1%. However, Q175F HET mice did not, and Q175FDN HET forebrains were significantly smaller than Q175F forebrains (Figure 7B, right panel). The cerebellum was relatively spared in both lines of mice with HET mice not showing any differences from WT mice. However, Q175F HOM mice showed significant cerebellar atrophy of 10.8% at 12 months of age and the remaining Q175FDN HOM mouse showed a similar reduction of 6% (Figure 7C).

Volumetric assessment of forebrain structures

Striatal, cortical, and corpus callosum volume was assessed using stereology. Q175FDN HOM mice displayed significant atrophy in all assessed forebrain regions as early as 3 months of age (Striatum 17.3% loss, cortex 13.4% loss, Corpus callosum 12.3% loss), with progressive loss to 12 months of age (Striatum 33% loss, cortex 28.2% loss, Corpus callosum 27% loss). Q175FDN HET mice displayed significant atrophy of the striatum from 6 months of age (4.5% loss progressing to 10% loss at 12 months) and the cortex and corpus callosum from 9 months of age (cortex 5.5% loss progressing to 7% loss by 12 months of age, corpus callosum 8.1% loss progressing to 8.6% loss by 12 months of age)(Figure 7D–F, left panels). At 12 months of age, Q175F HOM mice did have atrophy in all three forebrain regions (Striatum 20.7% loss, cortex 19.6% loss, Corpus callosum 22.4% loss). However, Q175FHET mice did not display these changes and Q175FDN HET mice had significantly smaller striata and corpus callosums than Q175F HET mice (Figure 7D–F, right panels). Taken together, these data indicate an acceleration or worsening of forebrain specific atrophy in Q175FDN mice with higher muHtt levels.

Brain histology

Striatal DARPP-32 immunoreactivity, a measure of healthy medium spiny neurons, was evaluated by integrated optical density (IOD) at 3, 6, 9, and 12 months of age in Q175FDN mice and at 12 months of age in Q175F mice. DARPP-32 IOD was significantly reduced in Q175FDN HOM striata from 6 months of age and in Q175FDN HET striata at 12 months of age (Figure 8A and B, left panel). At 12 months of age, Q175F HOM and HET mice also showed significant reductions in DARPP-32 IOD (Figure 8A and B, right panel). The magnitude of reduction in the one remaining Q175FDN HOM striata appeared to be greater than that in Q175F HOM striata. However, this did not reach significance

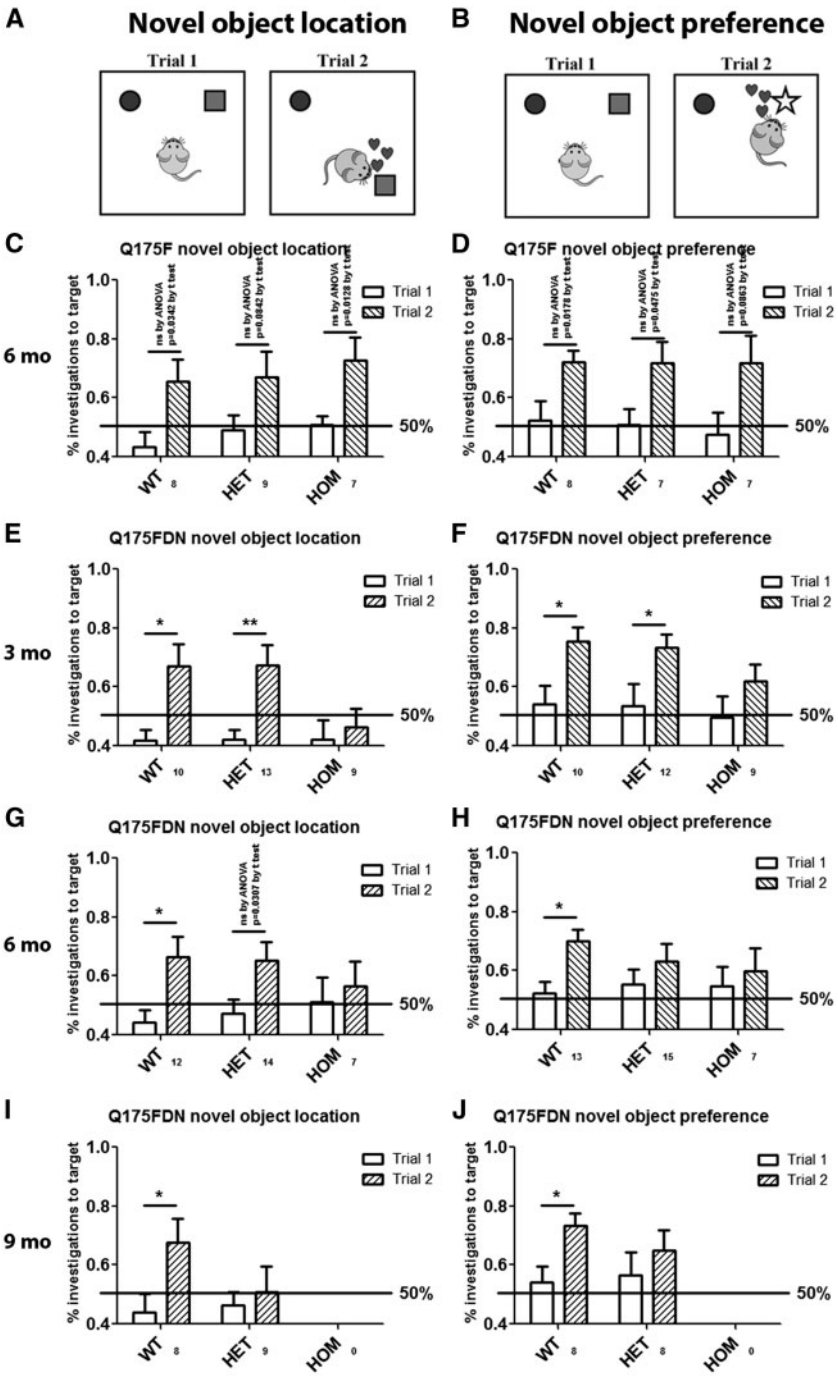

Figure 5. Q175FDN mice display progressive spatial and object recognition learning deficits. (**A**) Spatial learning was assessed by evaluating preference for a known object in a novel location. (**B**) Object recognition was assessed by evaluating preference for a novel object. (**C,D**) At 3 months of age, Q175FDN HOM mice display deficits in both learning tasks, while HET mice display no deficits. (**E,F**) At 6 months of age, Q175FDN HET mice maintained spatial learning, but display deficits in object recognition. (**G,H**) By 9 months of age, both HET and HOM Q175FDN mice were impaired in both learning tasks. (**I,J**) Conversely, Q175F HET and HOM mice display normal learning in both tasks at 6 months of age. *=difference between indicated columns, ns = not significant, *= $P < 0.05$, **= $P < 0.01$.

likely due to the *n* of 1. EM48 immunoreactivity, which is specific to aggregated human HTT (45), was used to evaluate muHtt inclusions at 3, 6, 9, and 12 months of age in Q175FDN mice and at 12 months of age in Q175F mice. The EM48 epitope is within HTT exon 1 just C-terminal to the proline rich region (46), thus the human sequence in present on the Q175 KI allele. Q175FDN HOM mice exhibited robust EM48 positive muHtt inclusions as early as 3 months of age. While some staining was apparent at 3 months of age in Q175FDN HET mice, robust inclusion deposition was not observed until 6 months of age (Figure 8C). At 12 months of age, robust EM48 positive inclusions were also observed in HET and HOM Q175F mice (Figure 8C). Comparison of Q175FDN HOM mice at 3, 6, and 9 months of age at low magnification demonstrates that inclusion deposition is cortical layer specific with projection layers II/III and V/VI showing more EM48 immunoreactivity at 3 months of age than non projection

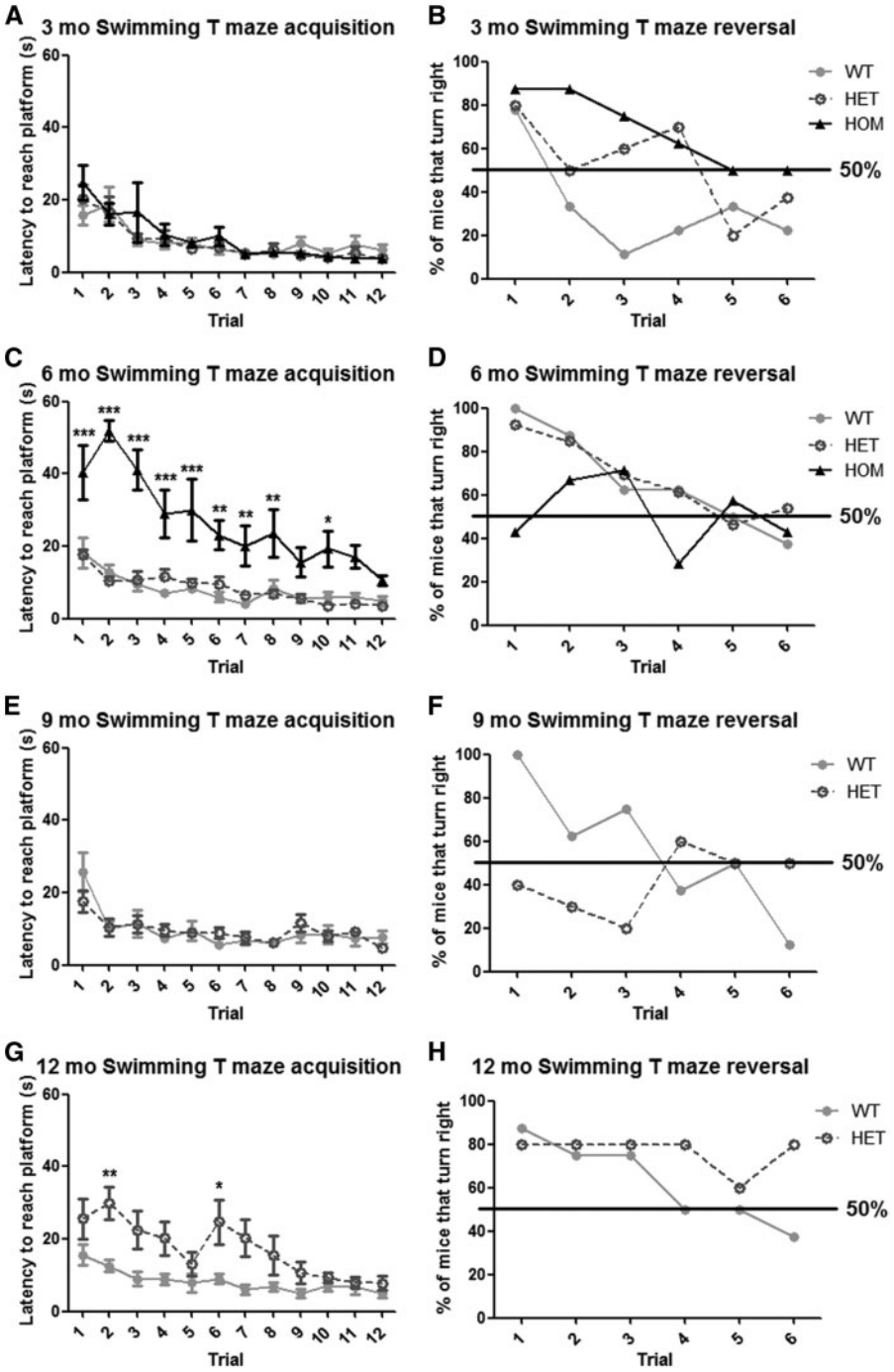

Figure 6. Q175FDN mice display progressive acquisition and reversal learning deficits in the swimming T maze. Mice were trained over four trials per day on 3 consecutive days to locate a submerged escape platform in the right arm of a water filled T maze and latency to reach the platform was scored. On day 5, the platform was moved to the left arm, and the percent of mice that turned into the right arm first was scored over 6 reversal learning trials. **(A,B)** At 3 months of age, there was no effect of genotype on acquisition, however, HET and HOM mice did not perform as well as WT mice in reversal learning. **(C,D)** By 6 months of age, HOM mice display significant acquisition and reversal learning deficits. **(E,F)** by 9 months of age, HET mice display normal acquisition, but impaired reversal learning. **(G,H)** At 12 months of age, HET mice display both acquisition and reversal learning deficits. *=different from WT, *= $P < 0.05$, **= $P < 0.01$, ***= $P < 0.001$.

layers I and IV. This pattern is still somewhat apparent at 6 months of age. However, by 9 months of age, inclusions are uniformly high throughout the brain (Figure 8D). Taken together, these results indicate that both lines of mice display HD-like brain histological changes.

Q175FDN mice exhibit early and robust HD-like striatal gene expression changes

Microdissected striata from 3-, 6- and 9-month old Q175FDN WT, HET, and HOM mice were evaluated for relative expression level of 5 genes known to be downregulated in HD caudate (47)

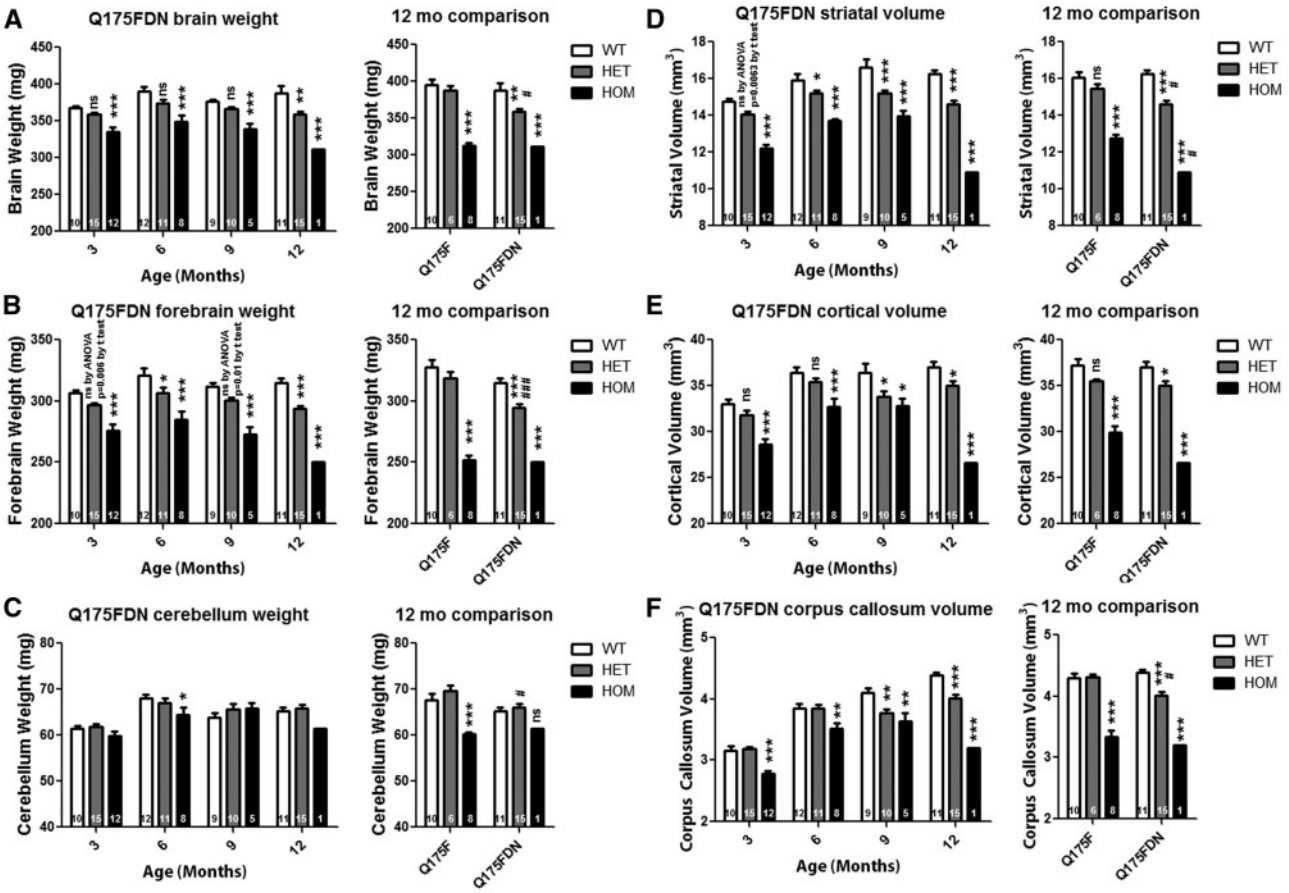

Figure 7. Q175F and Q175FDN mice display forebrain specific atrophy. Weights and structure volumes were assessed at 3, 6, 9, and 12 months of age in Q175FDN mice and at 12 months of age in Q175F mice. (**A**) Whole brain weight is reduced from 3 months of age in Q175FDN HOMs and at 12 months of age in Q175F HOMs. Q175FDN HET mice also showed reduced brain weight at 12 months of age, while Q175F HOM mice did not. (**B**) Forebrain weight is reduced in Q175FDN HET and HOM mice from 3 months of age, though to a greater degree in HOM mice, and at 12 months of age in Q175F HOMs, but not HETs. (**C**) The cerebellum is relatively preserved, though a reduction was observed at 6 months in Q175FDN HOM mice and at 12 months in Q175F HOM mice. (**D**) Striatal volume is reduced from 3 months of age in Q175FDN HET and, to a greater degree, HOM mice. At 12 months of age, striatal volume is reduced in Q175F HOM but not HET mice. (**E**) Cortical volume is reduced in Q175FDN HOM mice from 3 months of age and HET mice from 9 months of age. Conversely, cortical volume is reduced in Q175F HOM mice at 12 months of age, but not HET mice. (**F**) Corpus callosum volume is reduced in Q175FDN HOM mice from 3 months of age and HET mice from 9 months of age. Corpus callosum volume is reduced in 12 month Q175F HOM, but not HET mice. *=different from WT same age/line#=different from same genotype Q175F, ns = not significant, *= $P < 0.05$, **= $P < 0.01$, ***= $P < 0.001$.

and zQ175 striata (21); cannabinoid receptor 1 (Cnr1), glutamate transporter 1 (GLT1), dopamine- and cAMP-regulated neuronal phosphoprotein (DARPP-32), phosphodiesterae 10A (PDE10A), and dopamine receptor D2 (Drd2) (Figure 9). Striatal expression of Cnr1 and DARPP-32 was reduced in Q175DN HET and HOM mice from 3 months of age (Figure 9B and C), the earliest time point evaluated. At 3 months, Cnr1 expression was suppressed by 33 ± 8% in HET mice and 59 ± 2% in HOM mice (Figure 9B), and DARPP-32 expression was suppressed by 25 ± 9% in HET mice and 45 ± 3% in HOM mice (Figure 9C). By 9 months of age, the expression of both of these genes was suppressed by ∼50% in HET mice and ∼68% in HOM mice. GLT1, PDE10A, and Drd2 expression was normal in Q175FDN HET and HOM mice at 3 months of age, but reduced at 6 and 9 months of age (Figure 9D–F). At 9 months of age, GLT1 expression was suppressed by 28 ± 5% in HET mice and 23 ± 5% in HOM mice (Figure 9D), PDE10A expression was suppressed by 41 ± 6% in HET mice and 60 ± 6% in HOM mice (Figure 9E), and Drd2 expression was suppressed by 52 ± 6% in HET mice and 64 ± 3% in HOM mice (Figure 9F). Interestingly, while there was a trend toward greater magnitude reduction of Cnr1 expression in HOM striata compared to HET striata, it did not reach significance, and no differences were observed between HET and HOM mice for expression of GLT1, PDE10A, or Drd2, indicating that dysregulation of these genes in Q175FDN mice is a truly dominant phenotype.

Enhanced membrane excitability and reduced excitatory input in Q175FDN striatal neurons

We performed whole-cell patch-clamp electrophysiological recordings in acutely prepared brain slices at 3 and 9 months of age to test the characteristics and function of living striatal projection neurons (SPNs).

Excitability and membrane properties

We measured the SPNs' rheobase (minimum somatic current input required to fire action potentials) and frequency of action potentials at rheobase in order to examine their excitability (Figure 10A–C). We saw lower rheobase in both the Q175FDN HET and HOM SPNs than in the WT SPNs at both 3 and 9 months of age (Figure 10B). This suggests an increase in excitability in these cells. The rheobase of the HET and HOM cells was not different from one another, suggesting a truly dominant

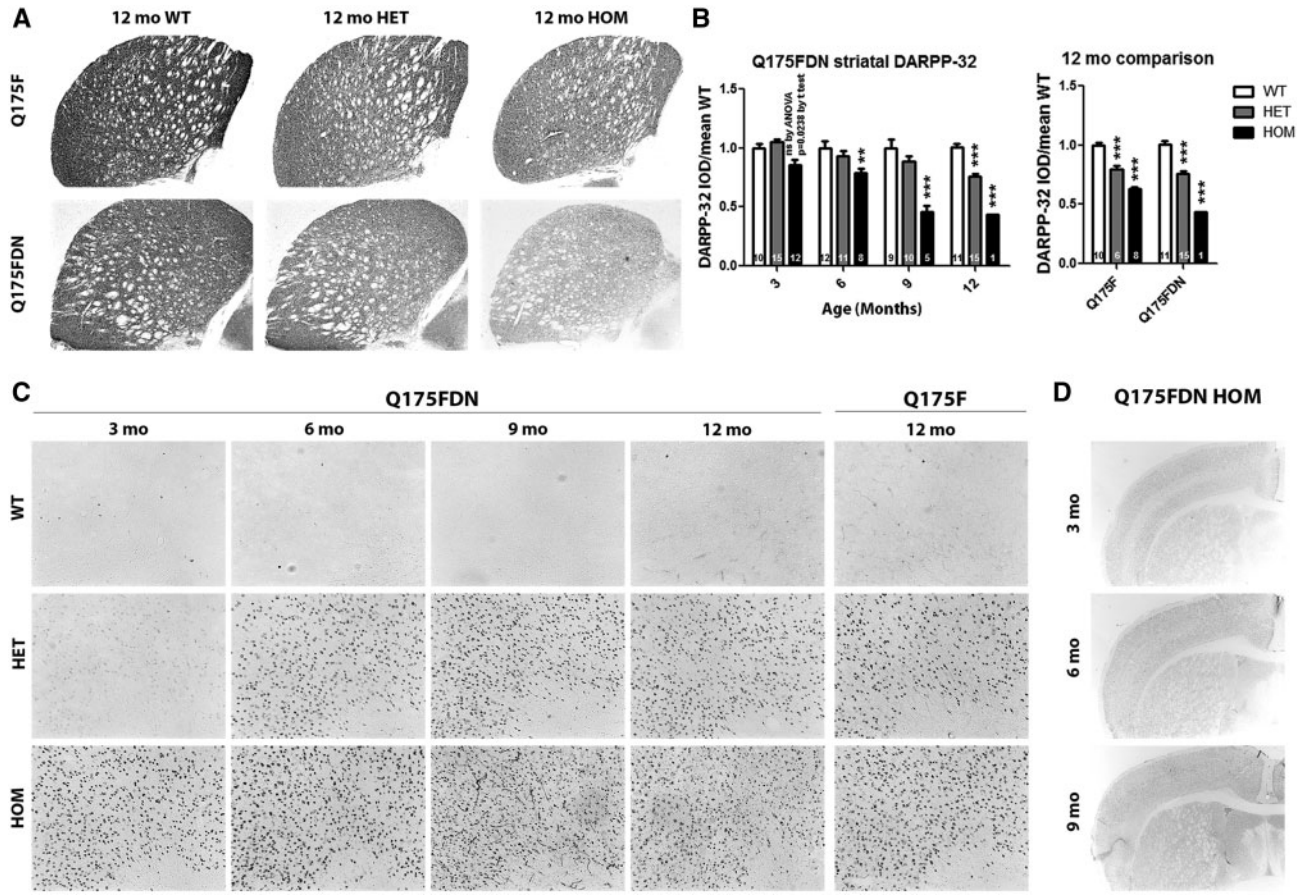

Figure 8. Q175F and Q175FDN mice display reduced striatal DARPP-32 and mutant Htt inclusions. Striatal DARPP-32 immunoreactivity and cortical EM48 positive Htt inclusions were assessed at 3, 6, 9, and 12 months of age in Q175FDN mice and at 12 months of age in Q175F mice. (**A**) Representative micrographs of DARPP-32 stained striata at 12 months of age. (**B**) Integrated optical density of striatal DARPP-32 immunoreactivity shows a decrease in Q175FDN HOM mice from 3 months of age and in HET and, to a greater degree, HOM mice of both lines at 12 months of age. (**C**) Q175FDN HET, and to a greater degree, HOM mice display EM48 positive cortical muHtt inclusions from as early as 3 months of age. Cortical muHtt inclusions were also observed at 12 months of age in Q175F HET and, to a greater degree, HOM mice. (**D**) Low magnification micrographs in Q175FDN HOM mice show that inclusion deposition is layer specific in younger mice, but more uniform throughout the cortex in older mice, indicating that deposition occurs earliest in specific cortical layers. *=different from WT same age/line, ns = not significant, **= $P < 0.01$, ***= $P < 0.001$.

phenotype, and there was no difference in rheobase frequency between genotypes (Figure 10C).

We also measured the current-voltage (I/V) curve in order to examine the change in membrane potential of the SPNs in response to somatic input current steps. At 3 months of age, there was a significant interaction between genotype and input current (*$P < 0.05$, Figure 10D (i); however, there was no significant difference between genotypes at any current step in *post hoc* analysis. At 9 months of age the HOM cells responded at all negative currents with a greater membrane potential change than the WT cells, and also responded at all negative currents except -50 pA with a greater voltage change than the HET cells (Figure 10D (ii). The HET cells tended to respond to negative currents with a greater membrane potential change than the WT cells, but this was not significant at any current. The progressive loss of the well-characterized rectification properties of SPNs (48) is consistent with what has been reported in other HD models (49). These changes may contribute to the above-mentioned increased excitability of the HOM and HET SPNs.

The resting membrane potential of the SPNs was also measured. There was no difference between genotypes in membrane potential at 3 months of age (Table 1), but at 9 months of age the HOM cells had a more depolarized resting membrane potential than the WT or HET cells (Table 1). This suggests changes to the membrane properties of the HOM SPNs that may also contribute to their increased excitability and altered I/V curve at 9 months of age. The altered resting membrane potential of SPNs from 9 month-old HOM Q175FDN mice may represent an end-stage phenotype, which the HET cells may develop at a more advanced age.

We also determined SPN membrane capacitance and input resistance by a 10mV depolarising step from membrane potential clamped at −70mV. At 3 months of age, the input resistance of HOM SPNs was higher than that of HET cells (Table 1). The HOM SPNs' membrane resistance at 9 months of age tended to be larger than that of both WT and HET SPNs, but this difference was not significant, mainly due to the large variability in this measure in WT and HET SPNs (Table 1). There was no difference in membrane capacitance between genotypes at either 3 or 9 months of age (Table 1).

Excitatory synaptic properties

In order to test the strength and/or number of excitatory synapses, we recorded spontaneous excitatory postsynaptic currents

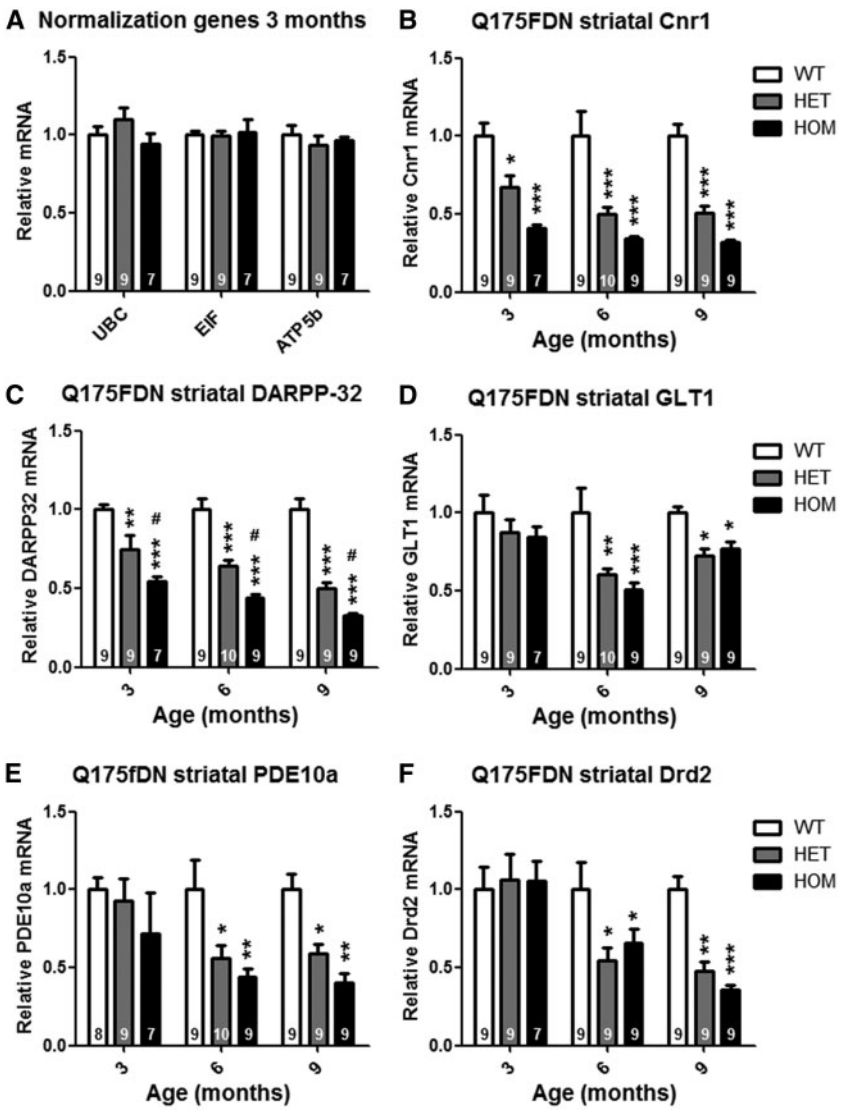

Figure 9. Q175FDN mice display progressive HD-like striatal gene expression changes. qRT-PCR was used to evaluate expression level of 5 HD-associated genes in striata of 3, 6, and 9 month old Q175FDN mice. (**A**) UBC, EIF, and ATP5b, which did not show any genotypic differences, were used as normalization genes. (**B**) Cannabinoid receptor 1 mRNA was reduced in Q175FDN HET, and to a greater degree, HOM striata from 3 months of age. (**C**) DARPP-32 mRNA was reduced in Q175FDN HET, and to a greater degree, HOM striata from 3 months of age. (**D**) Glutamate transporter I mRNA was reduced in Q175FDN HET and HOM mice from 6 months of age. (**E**) Phophodiesterase 10a mRNA was reduced in Q175FDN HET, and to a greater degree, HOM striata from 6 months of age. (**F**) D2 dopamine receptor mRNA was reduced in Q175FDN HET and HOM mice from 6 months of age. *=different from WT same age, #=different from HET same age, *= $P < 0.05$, **= $P < 0.01$, ***= $P < 0.001$.

(sEPSCs) from the SPNs (Figure 11A). HET Q175FDN SPNs had a significantly lower sEPSC frequency than WT SPNs at 3 months of age (Figure 11B, left panel); at 9 months of age, this reduced frequency was only a trend and not significant (Figure 11B, right panel). The sEPSC frequency of the HOM SPNs was significantly lower than that of WT cells at 9 months, and showed a tendency towards reduction at 3 months of age (Figure 11B). HOM and HET Q175FDN SPNs showed no significant difference in sEPSC frequency at either age, and there was no difference in sEPSC amplitude between any of the genotypes at 3 or 9 months of age (Figure 11B and C).

We also measured paired-pulse ratio (PPR) by evoking two EPSCs with a stimulating electrode placed dorsal to the recorded SPN with inter-stimulus intervals ranging from 50 to 500ms to detect changes in the presynaptic release probability at excitatory synapses (data not shown). There was a significant effect of interval (two-way ANOVA, *** $P < 0.0001$), but not of genotype (two-way ANOVA, $P = 0.0885$) or interaction between interval and genotype (two-way ANOVA, $P = 0.8880$) at 3 months of age ($n = 6$ WT, 5 HET and 4 HOM mice; $n = 11$ WT, 24 HET and 16 HOM cells). At 9 months of age, there was a significant effect of genotype (two-way ANOVA, *** $P < 0.0001$), but not of interval (two-way ANOVA, $P = 0.2829$) or interaction between interval and genotype (two-way ANOVA, $P = 0.9699$). The PPR of HET SPNs was higher than that of HOM SPNs at 50 ms (**$P < 0.01$) and 100 ms (*$P < 0.05$) intervals ($n = 5$ WT, 5 HET and 4 HOM mice; $n = 11$ WT, 12 HET and 13 HOM cells). This suggests a change in presynaptic release probability between Q175FDN genotypes, but there was no significant difference in PPR compared to WT. At 3 months of age, there was an effect of input current (two-way ANOVA, *** $P < 0.0001$), but not of genotype (two-way ANOVA, $P = 0.6936$) or interaction between genotype and input current (two-way ANOVA, $P = 1.0000$) on the size of evoked EPSCs with increasing stimulation intensity (input/output curve ($n = 6$ WT, 5 HET and 4

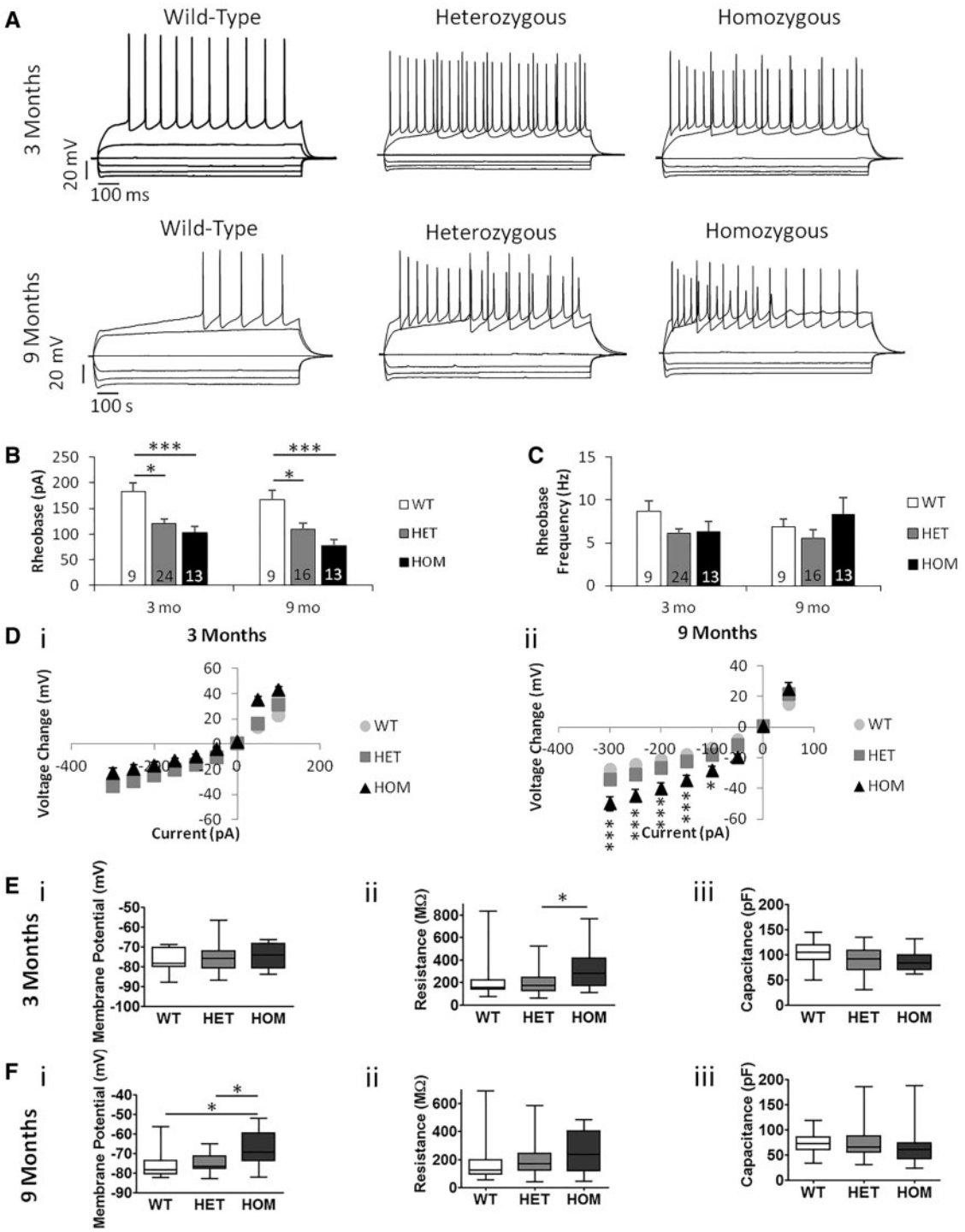

Figure 10. Q175FDN mice have more excitable MSNs. (**A**) Examples of I/V curve recordings from Q175FDN mice at 3 months and 9 months of age. At 3 months $n = 6$ WT, 5 HET, 4 HOM mice. At 9 months $n = 5$ WT, 5 HET, 4 HOM mice. Number of cells indicated on figure columns. (**B**) Rheobase. There was a significant effect of genotype on the rheobase at 3 ($P = 0.0005$) and 9 months ($P = 0.0007$). WT mice had a higher rheobase than HET and HOM at both 3 ($P < 0.05$, $P < 0.001$) and 9 months ($P < 0.05$, $P < 0.001$). There was no difference between HET and HOM at either age ($P > 0.05$). (**C**) Rheobase frequency. There was no difference between genotypes at 3 ($P > 0.05$) or 9 months ($P > 0.05$). (**D**) I/V curve. i) At 3 months there was a significant interaction between genotype and input current (*$P = 0.0124$) and of input current ($P < 0.0001$). There was no significant difference between genotypes at any specific input current ($P > 0.05$). ii) At 9 months there was a significant interaction of genotype and input current ($P < 0.0001$), and significant effects of genotype ($P < 0.0001$) and input current ($P < 0.0001$). The voltage of HOM mice changed more than WT and HET mice at -300 pA ($P < 0.001$), -250 pA ($P < 0.001$), -200 pA ($P < 0.001$), -150 pA ($P < 0.001$) and -100 pA ($P < 0.05$) inclusive.

HOM mice; $n = 8$ WT, 22 HET and 16 HOM cells). At 9 months of age, there was again an effect of input current (two-way ANOVA, *** $P < 0.0001$), but not of genotype (two-way ANOVA, $P = 0.2526$) or interaction between genotype and input current (two-way ANOVA, $P = 0.9999$; $n = 5$ WT, 5 HET and 4 HOM mice; $n = 12$ WT, 13 HET and 13 HOM cells; data not shown).

Table 1 Basic Membrane Properties of Q175 SPNs

	3 Months			9 Months		
Property	WT ($n = 9$)	HET ($n = 26$)	HOM ($n = 13$)	WT ($n = 10$)	HET ($n = 16$)	HOM ($n = 13$)
V_m (mV)	76.5 ± 2.1	75.5 ± 1.4	74.8 ± 1.8	75.8 ± 2.4	74.8 ± 1.3	66.8 ± 2.6*,#
R_m (MΩ)	228.0 ± 69.4	198.9 ± 20.0	307.0 ± 38.6#	181.7 ± 36.3	192.7 ± 22.9	249.9 ± 34.7
C_m (pF)	104.8 ± 8.1	89.6 ± 4.8	86.7 ± 4.2	72.2 ± 5.0	73.8 ± 6.3	64.4 ± 8.8

Sample sizes in parentheses. Sample means ± S.E.M. are presented.

*=different from WT $P < 0.05$.

#=different from HET $P < 0.05$.

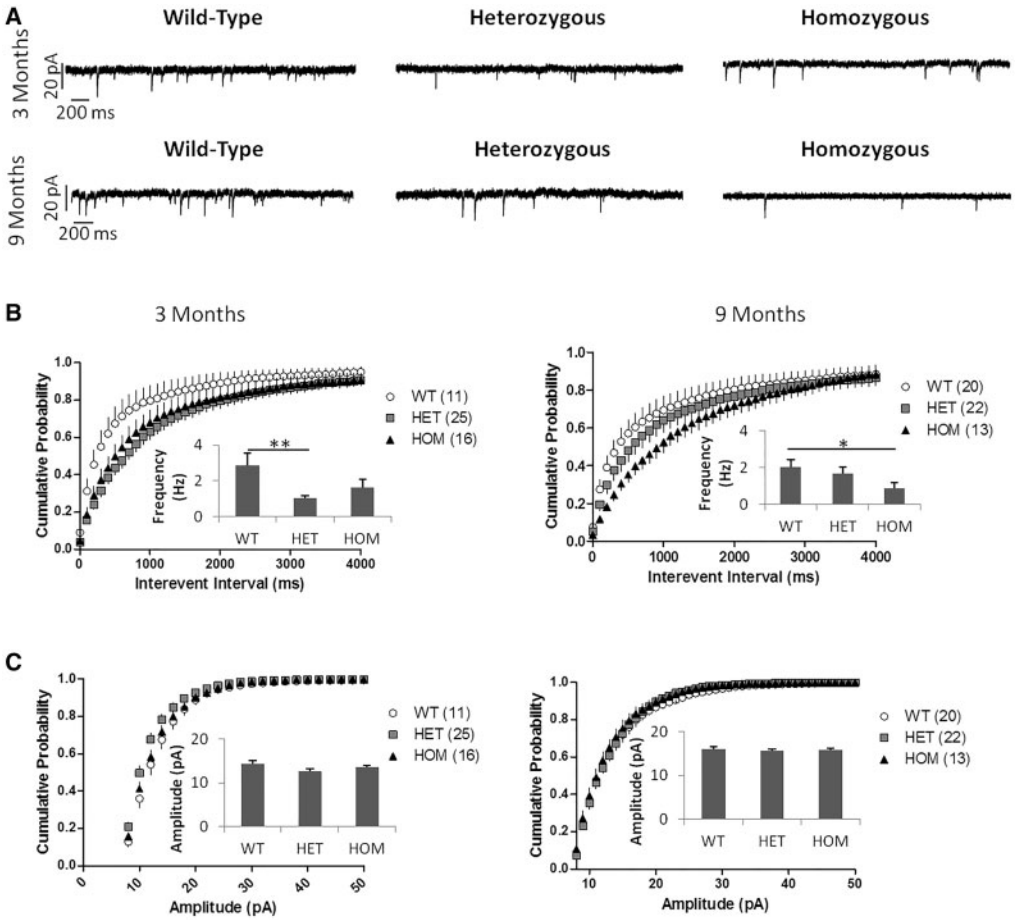

Figure 11. Q175 MSNs show decreased sEPSC frequency. (**A**) Example sEPSC recordings from Q175FDN mice at 3 and 9 months of age. At 3 months $n = 6$ WT, 5 HET, 4 HOM mice. At 9 months $n = 5$ WT, 5 HET, 4 HOM mice. Number of cells indicated next to genotype in figure legend. (**B**) sEPSC frequency cumulative probability and mean (inset). At 3 months there was a significant difference between groups ($P = 0.0045$). HET SPNs had lower sEPSC frequency than WT SPNs ($P < 0.01$). There was no difference between WT and HOM or between HET and HOM SPNs ($P > 0.05$). At 9 months there was also a significant difference between groups ($P = 0.0279$). HOM SPNs had lower sEPSC frequency at than WT SPNs ($P < 0.05$). There was no difference between WT and HET or between HET and HOM SPNs ($P > 0.05$). (**C**) sEPSC amplitude cumulative probability and mean (inset). There was no difference in sEPSC amplitude at 3 or 9 months of age. All mice shown were male. There was a significant effect of genotype and interevent interval on interevent interval cumulative probability at both 3 and 9 months ($P < 0.0001$ for both effects at both ages). There was no significant interaction of genotype and interevent interval at either age ($P > 0.05$) All data analysed using one- and two-way repeated measures ANOVAs with Bonferroni *post hoc* tests. * $P < 0.05$, ** $P < 0.01$.

Discussion

Transgene effects and muHtt levels

Genes that confer resistance to the antibiotic neomycin are often used for selection of transgene positive clones during gene targeting. However, the presence of the neo cassette can interfere with the expression of the transgene or neighbouring genes in the resulting transgenic mouse line (28,50). To overcome this, neo cassettes are typically floxed to allow cre-mediated excision of the cassette in the transgenic line. However, the neo selection cassette has been left in the transgene in several KI mouse models of HD despite previous reports of low Htt expression, abnormal development, and movement disorders in neo intact lines with expanded CAG compared to neo deleted lines (Table 2) (7,51). Aside from the disruption of Htt expression, the neo expression could have other unforeseen consequences on

Table 2. Knock-in mouse models of HD

Knock-in line(s)	Selection	Excision	HTT expression	Neo phenotypes
Q50(7)	pgk-neo	Yes/No	~33% w/neo	Aberrant brain development/perinatal lethality
CAG71,CAG94(12)	pgk-neo	No	Not reported	Not reported
Q20, Q50, Q92, Q111(11)	pgk-neo	Yes/No	10-50% w/neo [51]	Progressive movement disorder/lethality
Q72, Q80(9)	pgk-neo	Yes	Not reported	Not reported
CAG80, CAG150(10)	HPRT	Yes	Not reported	N/A
Q140(8)	pgk-neo	No	~35% w/neo [32]	Not reported
zQ175F(21)	pgk-neo	No	Not reported	Not reported

phenotype, further supporting excision. Neo excision from Q175F mice results in an approximately two-fold increase in muHtt protein in the brains of Q175FDN mice. Though expressed at a higher level than the Q175F KI allele, The Q175FDN KI allele is still hypomorphic, with total Htt protein levels equivalent to just over half the endogenous level. The residual reduction of the KI allele could be related to downregulation by the 54 base-pair insertion left upstream of the HTT locus after cre-mediated excision of the neo cassette. However, this sequence is small and unlikely to significantly interfere with Htt transcription. Residual reduction of the KI allele is more likely related to the highly expanded CAG tract. Expanded CAG mRNAs may be difficult to translate into long polyQ stretches due to depletion of available glutamine residues, and could result in ribosome stalling and activation of cellular mRNA quality control systems, such as no-go decay (52). This would result in a smaller proportion of expanded than non-expanded transcripts being translated and a subsequent reduction of expanded polyQ protein. Supporting this is the observation that expanded polyQ protein in neuronal progenitors differentiated from HD patient-derived induced pluripotent stem cells is ~65% of the level of the non expanded protein for a CAG 60 line but only ~20% of the level of the non-expanded protein for a CAG 180 line (53,54)(unpublished observation). Moreover, though reports of allelic HTT levels in adult-onset HD brain are inconsistent, finding the two alleles to be similar (55), the wtHTT level to be higher (56), or the muHTT level to be higher (57), a recent report found that muHtt protein is reduced in juvenile onset HD fibroblasts and brain (56) where CAG tract lengths more closely resemble KI mice. Thus, the reduction of highly expanded protein in Q175FDN mice may be consistent with HD.

Survival

zQ175 HOM mice have a mild survival deficit with onset at ~17.5 months of age and zQ175 HET mice do not display reduced survival (21). Consequently, the early, sudden death observed in the Q175F HET and HOM mice was unexpected. The slight drift in CAG tract length that occurred during back-crossing from zQ175 to Q175F is likely not sufficient to affect HD-like phenotypes. Moreover, even a substantial CAG tract expansion would not be expected to cause early onset fatal seizures in the absence of overt HD-like clinical signs. Thus, this phenotype is more likely related to Htt deficiency than to muHtt. The FVB/N background strain has natural susceptibility to seizures (58) that Htt protects against (manuscript submitted) possibly through its roles in axonal and vesicle transport and modulation of synatpic activity (59). Reduction of total Htt levels in Q175F mice increases susceptibility to and severity of seizures, resulting in sudden, early death from fatal seizures. These mice appear generally healthy up to the point of death. This is not a feature of HD, and restoration of KI muHtt by excision of the neo cassette rescues this phenotype in Q175FDN mice. Thus the Q175F mice appear to die from exacerbation of the FVB/N seizure phenotype as a result of Htt deficiency. Conversely, Q175FDN HET and HOM mice undergo a slow decline in health from 12 and 8 months of age, respectively, exhibiting increasing severity of HD-like clinical signs leading up to a humane endpoint. Though still partially hypomorphic on the KI allele, these mice appear to die from HD-like disease rather than Htt deficiency, making them a superior model of HD.

Peripheral pathology

zQ175 and Q175FDN mice display weight loss (Table 3), which is consistent with HD (33). Significant weight loss has been reported in zQ175 HET mice from 3 months of age and HOM mice from 1.5 months of age (21). After backcrossing to FVB/N, this phenotype was no longer significant in Q175F mice, though trends toward reduction were seen. This may be because FVB/N mice are larger than to C57BL/6 mice and a more substantial change is required to significantly impact body weight. After neo deletion and restoration of muHtt expression, significant body weight loss was observed in Q175FDN HET mice from 6 months of age and HOM mice from 3 months of age. These results suggest that Q175FDN mice are an appropriate model for investigations of muHtt-mediated metabolic dysfunction.

Testicular degeneration has not been reported in zQ175 mice, but it was observed in both Q175F and Q175FDN mice. The magnitude of testis weight loss was greater in Q175FDN mice with higher muHtt expression, indicating that this phenotype is directly tied to muHtt levels. Though Htt is expressed ubiquitously, the brain and the testes are the sites of highest expression (36). Histological evaluation revealed that seminipherous tubules were smaller in Q175FDN HOM testes compared to WT testes. This is consistent with HD, in which seminipherous tubule cross sectional area is reduced (36). Apoptotic degeneration was also noted in spermatogenic cells, which are reduced in number in HD testes (36), and in testosterone producing Leydig cells. Plasma testosterone is reduced in HD, and levels are inversely correlated with disease severity and dementia and directly correlated with total motor score (60), suggesting that Leydig cell pathology is also shared between HD and Q175FDN mice. Conversely, in YAC128 mice, the Leydig cells are relatively spared and Plasma testosterone levels are unchanged (36). Thus, Q175FDN mice may allow the study of aspects of HD-related testicular degeneration that could not previously be addressed.

Behaviour

zQ175, Q175F and Q175FDN mice all display the three classes of HD-like signs; motor deficits, psychiatric changes, and cognitive deficits (Table 3). The absence of motor deficits at 2 months of

Table 3. Comparison of onset age of HD-like phenotypes in Q175 knock-in HD mouse lines

	zQ175		Q175F		Q175FDN	
	HET	HOM	HET	HOM	HET	HOM
Survival deficit	none(21)	17.5 mo(21)	3 mo	3 mo	13 mo	9 mo
Body weight	3 mo(21)	1.5 mo(21)	ns	ns	6 mo	2 mo†
Testicular weight	ND	ND	12 mo†	12 mo†	9 mo	3 mo†
Rotarod	7 mo(21)	7 mo(21)	ns	4 mo	8 mo	6 mo
Climbing	none(21)	7.5 mo(21)	ns	8 mo	8 mo	8 mo
Grip strength	none(21)	1 mo†(21)	none	6 mo	9 mo	6 mo
hypoactivity	none(21)	8 mo(21)	none‡	none‡	none	9 mo
Open field anxiety	ND	ND	none‡	ns‡	9 mo	6 mo
Forced swim depression	ND	ND	9 mo	none	6 mo	3 mo†
Object location	ND	ND	none‡	none‡	9 mo	3 mo†
Object recognition	ND	ND	none‡	none‡	6 mo	3 mo†
Swimming acquisition	none(22)	10 mo(22)	ND	ND	12 mo	6 mo
Swimming reversal	ND	ND	ND	ND	9 mo	3 mo†
Whole brain atrophy	ns(22)	3 mo†(22)	none	12 mo†	12 mo	3 mo†
Forebrain atrophy	ND	ND	ns	12 mo†	6 mo	3 mo†
Striatal loss	4 mo(22)	3 mo†(22)	ns	12 mo†	6 mo	3 mo†
Cortical loss	4 mo(22)	3 mo†(22)	ns	12 mo†	9 mo	3 mo†
Corpus Callosum loss	ND	ND	none	12 mo†	6 mo	3 mo†
Cerebellum loss	ND	ND	none	12 mo†	none	6 mo
EM48 positive inclusions	6 mo(71)	ND	12 mo†	12 mo†	6 mo	3 mo†
DARPP-32 loss-protein	12 mo(71)	ND	12 mo†	12 mo†	12 mo	6 mo
DARPP-32 loss-mRNA	3 mo†(21)	3 mo†(21)	ND	ND	3 mo†	3 mo†
Cnr1 loss-mRNA	4 mo(21)	3 mo†(21)	ND	ND	3 mo†	3 mo†
GLT1 loss-mRNA	9.5 mo(21)	3 mo†(21)	ND	ND	6 mo	6 mo
PDE10a loss-mRNA	4 mo(21)	3 mo†(21)	ND	ND	6 mo	6 mo
Drd2 loss-mRNA	4 mo(21)	4 mo(21)	ND	ND	6 mo	6 mo
Increased SPN excitability	6–9 mo(22)	3–4 mo†(22)	ND	ND	3 mo†	3 mo†
Decreased SPN sEPSCs	7 mo(72)	7 mo(72)	ND	ND	3 mo†	9 mo

ND: not determined; ns: not significant (trend),

†=earliest time point evaluated,

‡Only evaluated at 6 mo, mo = months

age observed in Q175F and Q175FDN mice suggests that the motor phenotype of these lines is adult onset, unlike more severe N-terminal fragment models of HD, such as R6/2. This means that pre-symptomatic interventions for preventative studies of experimental therapeutics are possible in these lines. Unlike Q175F mice, Q175FDN mice also exhibit signs of anxiety-like and depressive-like psychiatric changes, consistent with HD. Additionally, the progressive cognitive deficits observed in Q175FDN mice were more severe than those previously reported for full-length models of HD. For example, in the swimming T-maze, reversal learning deficits were found to significantly precede acquisition learning deficits. This is consistent with YAC128 mice, which display late onset reversal learning deficits but normal acquisition learning in the swimming T-maze (42) and likely model an earlier phase of disease.

Neuropathology and striatal gene expression

The neuropathological changes observed in Q175FDN mice are consistent with HD brain and with what has been reported for other HD mouse models (43). Atrophy was observed in all evaluated forebrain regions. However, the magnitude of loss was greatest and the onset was earliest in the striatum, which is consistent with HD, in which the striatum is the region most susceptible to neurodegeneration and where the earliest changes occur (61). Whole brain atrophy in HOM mice and striatal and cortical loss in HET and HOM mice have previously been reported for the zQ175 line by MRI (22). No changes in whole brain weight were observed for zQ175 HET mice, unlike Q175FDN HET mice, indicating a worsening of phenotype in Q175FDN mice. Conversely, striatal and cortical atrophy were observed at an earlier time point in zQ175 HET mice than in Q175FDN mice. However, it is impossible to make a direct comparison between the lines because zQ175 mice were evaluated using MRI, while Q175F and Q175FDN mice were evaluated using stereology. It has been previously demonstrated that MRI is a more sensitive technique for volumetric analysis and is capable of detecting changes earlier than stereology (62). Therefore, it is likely that MRI evaluation of Q175FDN HET mice would demonstrate striatal and cortical loss at an earlier time point.

The early inclusion deposition observed in projection cortical layers II/III and V/VI as compared to non-projection layers I and IV in Q175FDN brain is consistent with these layers being most susceptible to muHtt-related changes. Projection layer-specific cortical thinning that has been previously reported in YAC128 brain (62), and cortical thinning in HD brain is greatest in projection layers III, V, and VI (63).

The striatal gene expression changes observed in Q175FDN mice are consistent with what has been observed in other mouse models of HD, including R6/2 (64), YAC128 (25), and zQ175 (21). Interestingly, while zQ175 mice display sexual dimorphism in gene expression changes with HOM females

displaying the earliest changes (21), no differences between male and female mice were observed in Q175FDN gene expression (data not shown). This may be due to acceleration of changes in Q175FDN mice. Sex differences were not apparent at later time points in zQ175 mice and the earliest time point for both studies was similar. This would mean that Q175FDN mice would be expected to be at a later disease stage than zQ175 mice at this time point.

Electrophysiology

The electrophysiological changes to Q175FDN SPNs seen here are generally similar to those seen in other HD mouse models such as R6/2, R6/1, YAC128 and Q175 (47,56–58), with decreased rheobase, reduced frequency of spontaneous activity and, in the case of the homozygotes, increased membrane resistance. Notably, in this model these alterations all occur by 3 months of age, prior to the time that the behavioural phenotype becomes apparent. The changes to rheobase and membrane resistance, as well as the altered I/V curve for homozygotes at 9 months, suggest a decrease in inwardly-rectifying K^+ currents as has been reported in the R6/2 model (47) and would be expected to increase SPN excitability. It is striking that most of the electrophysiological changes observed at 3 months of age are similar for heterozygotes and homozygotes, whereas by 9 months the homozygotes appear to be more affected. These findings are consistent with a report suggesting two copies of the mutant allele do not modify age of onset but may accelerate disease progression or increase the severity of disease in HD-affected individuals (65)

The reduction in spontaneous activity frequency most likely reflects a decrease in the total number of synapses (or increase in the proportion of silent synapses) as opposed to a change in presynaptic release probability, since no difference was observed between wild-type and Q175FDN in the paired-pulse ratio recorded from SPNs in response to cortical stimulation. The significant decrease in corpus callosum volume found by 3 months in homozygous and by 9 months in heterozygous Q175FDN mice indicates reduced intracortical connectivity and, as a reflection of more general loss in cortical white matter, also suggests diminished cortical input to the striatum; such changes would result in a decrease in functional excitatory synapses and contribute to a deficit in sEPSC frequency recorded from Q175FDN striatal SPNs. In addition, a reduction in the number of synapses would be consistent with the decrease in sEPSC frequency and spine density shown previously in Q175 SPNs (58), although the reduced frequency of sEPSCs found in our study was observed in heterozygous Q175FDN SPNs at 3 months, while other studies of Q175 SPNs showed reduced sEPSC frequency starting at 7 months of age (22,58). Overall, the increase in muHtt expression in Q175FDN mice may accelerate the electrophysiological phenotype.

Conclusions

Q175FDN mice display earlier and more robust HD-like phenotypes than the parent lines zQ175 and Q175F with a greater variety and magnitude of changes in HET animals (Table 3). In fact, the Q175FDN model displays the earliest and most robust HD-like phenotypes of any KI or full-length HD mouse model and the largest variety and greatest magnitude of HD-like phenotypes ever reported in a HET HD mouse. This allows for shorter preclinical testing intervals in a more relevant model. Additionally, many of the HD-like phenotypes of Q175FDN mice, including striatal gene expression changes and electrophysiological SPN changes, appear to be truly dominant; a feature consistent with human HD that is not common to other HD mouse models. Thus, Q175FDN mice more faithfully genetically and phenotypically recapitulate human HD than any previously reported mouse model.

While backcrossing to the FVB/N background strain did enhance many HD-like phenotypes, there are caveats to consider with any mouse line on this background strain. Mice on the FVB/N strain undergo retinal neurodegeneration (66), so Q175FDN mice may not be suitable for some forms of cognitive testing that require sight, such as touch screen or light cued learning assays (67,68). Though less obvious than the sudden early death phenotype of Q175F mice, the zQ175 mice may exhibit Htt deficiency effects confounding studies of Huntington disease. Thus, for studies involving sight cued learning assays, the zQ175 line with the neo cassette excised may be preferable. However, it remains to be seen if the early and robust phenotypes of the Q175FDN HET mice would be as apparent on the C57BL/6 background, which has previously been shown to be less susceptible to HD-like neurodegeneration (23,24). Nonetheless, Q175FDN mice are a superior mouse model of HD and, excepting cases where experimental design requires sight or where elements specific to human HTT are under study, should be the preferred model for preclinical studies of HD.

Materials and Methods

Mice and breeding

Mice were maintained under a 12-h light:12-h dark cycle in a clean facility and given free access to food and water. Experiments were performed with the approval of the animal care committee of the University of British Columbia. zQ175 mice on the C57BL/6 background (21) were obtained from JAX and the CHDI foundation. Genotyping for the transgene by the presence of the neo cassette or the WT *Hdh* allele was performed as in (12). Mice were backcrossed 10 generations to the FVB/N strain by crossing male zQ175 HET mice with female FVB/N mice to generate Q175F mice. CAG sizing modified from (17) as in (69) was used to verify that breeders remained within the normal range for the line of around 200.

For deletion of the neo cassette, male Q175F HETs were crossed to Vasa-cre females also on the FVB/N background strain (30) (JAX). Vasa-cre mice express cre recombinase in germline cells resulting in global recombination in progeny when female Vasa-cre breeders are used. *Hdh* and neo genotyping, CAG sizing, and genotyping for the cre recombinase (JAX Generic Cre standard PCR protocol) were used to identify progeny positive for the expanded CAG allele and the *Hdh* allele, and negative for the neo cassette and the cre recombinase. The selected Q175FDN HET mice were intercrossed and progeny were genotyped as WT, HET, or HOM using the *Hdh* and CAG sizing assays. Direct sequencing of the promoter region of the KI allele was then compared in Q175F and Q175FDN HOM mice using primers recognizing sequences adjacent to the floxed neo cassette (F: GTGAGAGCTAGCACTGGCA, R: CAAAACCGTTCCGGCTTCAG, Neo_F: GATCGGCCATTGAACAAGATG, Neo_R: AGAGCAGCCGA TTGTCTGTTG) to verify excision and the presence of the remaining loxp sequence.

HTT level assessment

Four-month old WT, HET, and HOM mice from the Q175F and Q175FDN lines were killed with an overdose of 2.5% Avertin IP.

Brains were removed, chilled briefly on ice, and microdissected by region. Right cortices and both striata from an n of 4 mice per genotype per line were used for Htt quantitation by allelic separation immunoblotting as previously described (35). Htt level in WT mice did not differ between the two lines, so quantitative data from WT mice was combined into a single group.

Longevity assessment

Longevity cohorts were housed with behavioural cohorts and received longitudinal behaviour testing to normalize any effects of enrichment. Mice were observed daily and weighed monthly. After the onset of clinical signs, including ataxia, weight loss, piloerection, and postural changes, mice were given additional nesting material and food and hydrogel on the cage floor to facilitate access. Mice exhibiting clinical signs were monitored daily for signs that they had reached a humane endpoint, such as loss of the righting reflex, limb paralysis, gasping breathing, or persistent seizures, at which time they were euthanized by CO_2 asphyxiation. At 12 months of age, surviving Q175F mice were collected for neuropathological evaluation. Q175FDN longevity assessment continued until 18 months of age, a time at which all transgenic mice had reached a humane endpoint.

Behaviour testing

Longitudinal accelerating rotarod was performed as in (35). Briefly, two-month old mice were trained over 3 120s trials per day for 3 days on an 18 rpm fixed speed rotarod. Mice that fell were returned immediately to the rod. The mean latency to the first fall and mean falls for the three trials were scored. Mice were tested at 2 month intervals from 2 to 12 months of age over 3 300s trials on an accelerating rotarod (5–40 rpm). The mean latency to fall for the 3 trials was scored.

Longitudinal climbing was performed as in (35). Briefly, mice were tested at 2 month intervals from 2–12 months of age during a 5 min exploration of an inverted wire pencil holder on the bench top. latency to begin climbing (all four feet off of the bench top) and total time spent climbing were scored.

Longitudinal forelimb grip strength was measured using a Columbus Instruments force meter. The mice were allowed to grip a wire mesh with their forelimbs and gentle backward pressure was applied until the mouse released the mesh. The peak force applied was averaged for three trials and values were normalized to the mean value for WT mice tested at the same age within the same cohort.

Open field exploration and object learning were performed as in (35). Briefly, mice were placed in a 50x50 cm open top box under bright lighting and recorded via ceiling mounted video camera during a 10 min exploration. Distance travelled and time spent in the centre of the field were scored as measures of activity and anxiety, respectively, using Ethovision XT 7 animal tracking software (Noldus). After a 5 min inter-trial interval (ITI), mice were returned to the box, now containing 2 objects in the upper corners of the box between which mice have previously shown no baseline preference. After a 5-min exploration, mice were given a 5 min ITI during which the right hand object was moved to the lower corner. The mice were then given another 5 min exploration. Investigations to the target object on the right were scored using Ethovision XT 7 as a measure of spatial learning. On the following day mice were returned to the box for a 5 min acclimation, given a 5 min ITI, and then allowed to explore the box for 5 min with the same 2 objects now back in their original positions. After a 5 min ITI, the object on the right was replaced with a novel object and the mice were given another 5 min exploration. Investigations to the target object on the right were scored using Ethovision XT 7 as a measure of object recognition. Data for any mouse that failed to investigate both objects was excluded. Each mouse received this testing only once and multiple cohorts were used to generate data from different ages.

A modified Porsolt forced swim test was performed as in (40). Briefly, mice were placed in transparent cylinders filled with room temperature water for 6 min. A video camera was used to record activity from the side. Time spent immobile was scored for the final 5 min of the trial. Each mouse received this testing only once and multiple cohorts were used to generate data from different ages. Due to the stressful nature of this test it was the final behaviour test performed for each group of mice.

Swimming T-maze testing was performed as in (70). Briefly, a T-maze filled with water and an escape platform beneath the surface at the end of the right arm of the maze was used. For acquisition, mice were placed at the base of the T and latency to reach the platform and first arm entry (R or L) were scored over 4 trials per day with a 45 min ITI for 3 days. The mice were then given 1 day to rest. On day 5 reversal learning was assessed by moving the escape platform to the left arm of the maze and scoring latency to reach the platform and first arm entered over 6 trials with a 45 min ITI. Mice receiving this testing did not receive any other behaviour testing and were not used for histological or biochemical analyses.

Neuropathology and histology

Mice were anaesthetized with 2.5% Avertin IP followed by transcardiac perfusion with phosphate buffered saline (PBS) and 4% paraformaldehyde (PFA). Brains and testes were removed and post-fixed in 4% PFA in PBS for 24 hrs at 4°C. The following day testes were weighed and brains and testes were cryoprotected in 30% sucrose with 0.01% sodium azide. Once equilibrated, brains were weighed whole, divided into the forebrain and cerebellum, and weighed again. Forebrains were then frozen on dry ice, mounted in Tissue-TEK O.C.T. embedding compound (Sakura), and cut via cryostat (Leica CM3050S) into a series of 25 μm coronal sections free-floating in PBS with 0.01% sodium azide.

Stereological volumetric analysis was performed as in (35). Briefly, a series of sections spaced 200 μm apart and spanning the striatum were stained for NeuN (1:1000, Millipore) using biotinylated anti-mouse secondary antibody (1:1000, Vector Laboratories), the ABC Elite Kit (Vector) to amplify signal, and 3,3'-diaminobenzidine (DAB, Thermo Scientific) detection. Structures were traced using Stereo Investigator software (MBF Bioscience) and volumes determined using the Cavalieri principle.

Striatal DARPP-32 integrated optical density was assessed as in (35). Briefly, a series of 4 mid-striatal sections were stained for DARPP-32 (1:500, R&D Systems) using biotinylated goat anti-rat secondary antibody (1:1000, Vector), the ABC Elite Kit, and DAB detection. Sections were imaged with a 5x objective (Zeiss) using a Zeiss Axioplan 2 microscope and Coolsnap HQ Digital CCD camera (Photometrics, Tucson, AZ, USA) and MetaMorph software (Molecular Devices). Staining intensity and integrated optical density were determined using ImageJ software. Values were normalized to the mean value for WT mice from the same age and cohort.

For qualitative evaluation of Htt inclusions, a mid-striatal section was incubated in EM48 (1:100, Millipore) anti-HTT primary antibody for 24h overnight. Sections were then washed and incubated with biotinylated goat anti-mouse secondary antibody (1:500, Vector), the ABC Elite Kit, and visualized with DAB. Images were taken as above, with 2.5× or 20× objectives (Zeiss).

Testes were cut in half at the transverse median and embedded in Tissue-TEK O.C.T. embedding compound. Testes were cut into 10 μm transverse sections via cryostat and dried onto charged glass slides (Fisher Scientific). Apoptotic cells were visualized by TUNEL using a POD In Situ cell death kit (Roche) according to the manufacturer's instructions. Sections were imaged using an Olympus Ix50 microscope with 2.5×, 20×, or 40× objectives (Zeiss) and Exi Aqua camera (QImaging).

Striatal gene expression

An *n* of 7–10 mice per age per genotype were killed with an overdose of 2.5% Avertin IP. Brains were removed, placed on ice briefly to increase tissue rigidity, and microdissected by region. Total RNA was isolated from both striata using Qiagen's RNeasy kit. 500ng of total RNA was reversed transcribed to cDNA using SuperScript III reverse transcriptase (Thermo Fisher) according to the manufacturer's instructions. The expression level of HD-associated striatal genes was evaluated as in (21). Briefly, 0.25 μl of cDNA was amplified using FastStart Universal Probe Master (Rox)(Roche), Universal Probe Library probe (Roche), and gene-specific primer, using an ABI 7500 Fast Real-Time PCR System (Applied Biosystems). The mean of the Ct values from triplicate wells was assessed for each sample. The relative quantity of target genes was normalized to the mean quantity for 3 housekeeping genes; ATP5b, EIF4A2, and Ubc, for which no genotype specific effects were observed. Values were then normalized to the mean value for WT mice of the same age.

Electrophysiology

Slice preparation: Animals were deeply anaesthetized with halothane vapour, decapitated, and the brain was rapidly removed. Brains were incubated in ice-cold artificial cerebrospinal fluid (aCSF; with Ca:Mg at 1:5 mM) equilibrated with 95% O2/5% CO_2 and cut on a vibratome (Leica VT1000) to make coronal slices (300 μm). Slices were transferred to a holding chamber with aCSF (Ca:Mg 2:1 mM) at 37°C containing (in mM): 125 NaCl, 2.5 KCl, 25 $NaHCO_3$, 1.25 NaH_2PO_4, 1 $MgCl_2$, 2 $CaCl_2$, 25 glucose, pH 7.3–7.4, 305–310 mosmol L-1 for 45 min then maintained at room temperature. In the recording chamber, slices were continually superfused at room temperature with oxygenated aCSF at 1–2 mL/min containing picrotoxin (50 μM, dissolved directly into aCSF, Tocris Bioscience) to block GABAA receptor-mediated inhibitory responses.

Whole-Cell Recordings: Pipettes (3–5 MΩ) were made from borosilicate glass capillaries using a Narishige micropipette puller (Narishige International). The intracellular solution was K±based as follows (mM): 145 potassium gluconate, 1 $MgCl_2$, 2 MgATP, 0.5 NaGTP, 1 EGTA, 10 HEPES, pH 7.25, osmolarity 290 mOsm. In all experiments, cells were rejected if access resistance exceeded 25 MΩ. All recordings were made using the whole-cell patch clamp technique with an Axopatch-200A and PatchClamp 10 software digitized at 20 kHz and filtered at 1 or 10 kHz.

Spontaneous Excitatory Postsynaptic Currents (sEPSC): Cells were voltage-clamped at −70 mV, with a 50 ms step to −80 mV every 30 s. Cells were rejected if background noise during recording exceeded 8 pA or if holding current was greater than −100 pA.

I/V Curve: Cells were current-clamped at 0 pA. For each sweep of the protocol, cells were maintained at 0 pA for 100 ms, held at a test current for 1000 ms, and returned to 0 pA for 400 ms. The test current was −300 pA on the first sweep and was made more positive by 50 pA on each subsequent sweep up to 250 pA. Cells were rejected if resting membrane potential was greater than −55 mV or if the shape of the response to current injection was not consistent with that of a spiny projection neuron (SPN).

Input/Output Curve: Cells were voltage-clamped at −70 mV. Activity was elicited by injecting current through a glass micropipette electrode filled with aCSF and positioned ∼150 μm dorsal to the site of recording. Pulses [duration of pulse] were delivered at 50, 100, 200, 300, 400 and 500 μA. Three sweeps were performed at each pulse amplitude and averaged for analysis.

Paired-Pulse Ratio: Cells were voltage-clamped at −70 mV. Activity was elicited by injecting current through a glass micropipette electrode filled with aCSF and positioned ∼150 μm dorsal to the site of recording. Pulses were administered at the current which elicited a half-maximal response in the input/output curve. Two pulses were administered per run with an interval of 50, 100, 250 or 500 ms between them. Three runs were performed for each interval length and were averaged for analysis. The paired-pulse ratio for each interval length was determined by dividing the average response amplitude to the second pulse by the average response amplitude to the first pulse to determine whether, on average, the response size had increased, decreased or remained the same.

Statistical analysis

WT mice exhibiting a reactive phenotype as determined by abnormal brain morphology (enlarged triangular forebrain and total brain weight over 500 mg) were excluded from analysis. Data are expressed as mean ± SEM unless otherwise noted. Analyses were performed using one- or two-way-ANOVA and Bonferroni *post hoc* tests (significance markers on figures) unless otherwise noted. Differences were considered statistically significant for $P < 0.05$. In cases where significance was not observed by ANOVA, but a strong trend was present, the *P* value for pairwise comparison by Student's *t*-test is reported on the figure. For single time point tests conducted after mice began to die (3 months of age) leading to unequal group size, *n* is reported in the figure.

Supplementary Material

Supplementary Material is available at *HMG* online.

Acknowledgements

The authors thank Vanessa Wheeler for CAG sizing protocols, Mark Wang and Mahsa Amirabbasi for excellent animal care, Shaun Sanders and Crystal Doty for assistance optimizing allelic separation immunoblotting, Niels Skotte for assistance optimizing qRT-PCR.

Conflict of Interest statement. None declared.

Funding

This work was supported by a grant from the CHDI foundation and the Canadian Institutes of Health Research (CIHR; FDN-143210). A.L.S. held postdoctoral fellowships from the Huntington Society of Canada, the CIHR and the Michael Smith Foundation for Health Research. A.S.D. holds a UBC four-year fellowship award and CIHR Canada Graduate Scholarship Doctoral award. M.P.P held a CIHR postdoctoral fellowship. M.R.H. is a University Killam Professor and the Canada Research Chair in Human Genetics and Molecular Medicine.

References

1. Evans, S.J.W., Douglas, I., Rawlins, M.D., Wexler, N.S., Tabrizi, S.J. and Smeeth, L. (2013) Prevalence of adult Huntington's disease in the UK based on diagnoses recorded in general practice records. *J. Neurol. Neurosurg. Psychiatry*., **84**, 1156–1160.
2. Fisher, E.R. and Hayden, M.R. (2014) Multisource ascertainment of Huntington disease in Canada: Prevalence and population at risk. *Mov. Disord*., **29**, 105–114.
3. Ross, C.A. and Tabrizi, S.J. (2011) Huntington's disease: from molecular pathogenesis to clinical treatment. *The Lancet Neurol*., **10**, 83–98.
4. Shannon, K.M. and Fraint, A. (2015) Therapeutic advances in Huntington's Disease. *Mov. Disord*., **30**, 1539–1546.
5. The Huntington's Disease Collaborative Research Group(1993) A novel gene containing a trinucleotide repeat that is expanded and unstable on Huntington's disease chromosomes. *Cell*, **72**, 971–983.
6. Andrew, S.E., Goldberg, Y.P., Kremer, B., Telenius, H., Theilmann, J., Adam, S., Starr, E., Squitieri, F., Lin, B., Kalchman, M.A., *et al.* (1993) The relationship between trinucleotide (CAG) repeat length and clinical features of Huntington's disease. *Nat. Genet*., **4**, 398–403.
7. White, J.K., Auerbach, W., Duyao, M.P., Vonsattel, J.P., Gusella, J.F., Joyner, A.L. and MacDonald, M.E. (1997) Huntingtin is required for neurogenesis and is not impaired by the Huntington's disease CAG expansion. *Nat. Genet*., **17**, 404–410.
8. Menalled, L.B., Sison, J.D., Dragatsis, I., Zeitlin, S. and Chesselet, M.F. (2003) Time course of early motor and neuropathological anomalies in a knock-in mouse model of Huntington's disease with 140 CAG repeats. *J. Comp. Neurol*., **465**, 11–26.
9. Shelbourne, P.F., Killeen, N., Hevner, R.F., Johnston, H.M., Tecott, L., Lewandoski, M., Ennis, M., Ramirez, L., Li, Z., Iannicola, C., *et al.* (1999) A Huntington's Disease CAG Expansion at the Murine Hdh Locus Is Unstable and Associated with Behavioural Abnormalities in Mice. *Hum. Mol. Genet*., **8**, 763–774.
10. Lin, C.H., Tallaksen-Greene, S., Chien, W.M., Cearley, J.A., Jackson, W.S., Crouse, A.B., Ren, S., Li, X.J., Albin, R.L. and Detloff, P.J. (2001) Neurological abnormalities in a knock-in mouse model of Huntington's disease. *Hum. Mol. Genet*., **10**, 137–144.
11. Wheeler, V.C., Auerbach, W., White, J.K., Srinidhi, J., Auerbach, A., Ryan, A., Duyao, M.P., Vrbanac, V., Weaver, M., Gusella, J.F., *et al.* (1999) Length-Dependent Gametic CAG Repeat Instability in the Huntington's Disease Knock-in Mouse. *Hum. Mol. Genet*., **8**, 115–122.
12. Levine, M.S., Klapstein, G.J., Koppel, A., Gruen, E., Cepeda, C., Vargas, M.E., Jokel, E.S., Carpenter, E.M., Zanjani, H., Hurst, R.S., *et al.* (1999) Enhanced sensitivity to N-methyl-D-aspartate receptor activation in transgenic and knockin mouse models of Huntington's disease. *J. Neurosci. Res*., **58**, 515–532.
13. Reddy, P.H., Williams, M., Charles, V., Garrett, L., Pike-Buchanan, L., Whetsell, W.O., Miller, G. and Tagle, D.A. (1998) Behavioural abnormalities and selective neuronal loss in HD transgenic mice expressing mutated full-length HD cDNA. *Nat. Genet*., **20**, 198–202.
14. Gray, M., Shirasaki, D.I., Cepeda, C., André, V.M., Wilburn, B., Lu, X.H., Tao, J., Yamazaki, I., Li, S.H., Sun, Y.E., *et al.* (2008) Full-length human mutant huntingtin with a stable polyglutamine repeat can elicit progressive and selective neuropathogenesis in BACHD mice. *J. Neurosci*., **28**, 6182–6195.
15. Slow, E.J., van Raamsdonk, J., Rogers, D., Coleman, S.H., Graham, R.K., Deng, Y., Oh, R., Bissada, N., Hossain, S.M., Yang, Y.Z., *et al.* (2003) Selective striatal neuronal loss in a YAC128 mouse model of Huntington disease. *Hum. Mol. Genet*., **12**, 1555–1567.
16. Hodgson, J.G., Agopyan, N., Gutekunst, C.A., Leavitt, B.R., LePiane, F., Singaraja, R., Smith, D.J., Bissada, N., McCutcheon, K., Nasir, J., *et al.* (1999) A YAC Mouse Model for Huntington's Disease with Full-Length Mutant Huntingtin, Cytoplasmic Toxicity, and Selective Striatal Neurodegeneration. *Neuron*, **23**, 181–192.
17. Mangiarini, L., Sathasivam, K., Seller, M., Cozens, B., Harper, A., Hetherington, C., Lawton, M., Trottier, Y., Lehrach, H., Davies, S.W., *et al.* (1996) Exon 1 of the HD gene with an expanded CAG repeat Is sufficient to cause a progressive neurological phenotype in transgenic mice. *Cell*, **87**, 493–506.
18. Schilling, G., Becher, M.W., Sharp, A.H., Jinnah, H.A., Duan, K., Kotzuk, J.A., Slunt, H.H., Ratovitski, T., Cooper, J.K., Jenkins, N.A., *et al.* (1999) Intranuclear inclusions and neuritic aggregates in transgenic mice expressing a mutant N-terminal fragment of huntingtin. *Hum. Mol. Genet*., **8**, 397–407.
19. Brooks, S.P. and Dunnett, S.B. (2015) Mouse Models of Huntington's Disease. In Nguyen, P.H.H.nd Cenci, A.M. (eds.), *Behavioral Neurobiology of Huntington's Disease and Parkinson's Disease*. Springer Berlin Heidelberg, Berlin, Heidelberg, pp. 101–133.
20. Pouladi, M.A., Morton, A.J. and Hayden, M.R. (2013) Choosing an animal model for the study of Huntington's disease. *Nat. Rev. Neurosci*., **14**, 708–721.
21. Menalled, L.B., Kudwa, A.E., Miller, S., Fitzpatrick, J., Watson-Johnson, J., Keating, N., Ruiz, M., Mushlin, R., Alosio, W., McConnell, K., *et al.* (2012) Comprehensive Behavioral and Molecular Characterization of a New Knock-In Mouse Model of Huntington's Disease: zQ175. *PLoS ONE*, **7**, e49838.
22. Heikkinen, T., Lehtimaki, K., Vartiainen, N., Puolivali, J., Hendricks, S.J., Glaser, J.R., Bradaia, A., Wadel, K., Touller, C., Kontkanen, O., *et al.* (2012) Characterization of Neurophysiological and Behavioral Changes, MRI Brain Volumetry and 1H MRS in zQ175 Knock-In Mouse Model of Huntington's Disease. *PLoS ONE*, **7**, e50717.
23. Van Raamsdonk, J.M., Metzler, M., Slow, E., Pearson, J., Schwab, C., Carroll, J., Graham, R.K., Leavitt, B.R. and Hayden, M.R. (2007) Phenotypic abnormalities in the YAC128 mouse model of Huntington disease are penetrant on multiple genetic backgrounds and modulated by strain. *Neurobiol. Dis*., **26**, 189–200.
24. Mantovani, S., Gordon, R., Li, R., Christie, D.C., Kumar, V. and Woodruff, T.M. (2016) Motor deficits associated with Huntington's disease occur in the absence of striatal degeneration in BACHD transgenic mice. *Hum. Mol. Genet*., pii: ddw050. [Epub ahead of print].

25. Pouladi, M.A., Stanek, L.M., Xie, Y., Franciosi, S., Southwell, A.L., Deng, Y., Butland, S., Zhang, W., Cheng, S.H., Shihabuddin, L.S., *et al.* (2012) Marked differences in neurochemistry and aggregates despite similar behavioural and neuropathological features of Huntington disease in the full-length BACHD and YAC128 mice. *Hum. Mol. Genet.*, **21**, 2219–2232.
26. Southwell, A.L., Ko, J. and Patterson, P.H. (2009) Intrabody gene therapy ameliorates motor, cognitive, and neuropathological symptoms in multiple mouse models of Huntington's disease. *J. Neurosci.*, **29**, 13589–13602.
27. Gogliotti, R.G., Lutz, C., Jorgensen, M., Huebsch, K., Koh, S. and DiDonato, C.J. (2011) Characterization of a commonly used mouse model of SMA reveals increased seizure susceptibility and heightened fear response in FVB/N mice. *Neurobiol. Dis.*, **43**, 142–151.
28. Pham, C.T.N., MacIvor, D.M., Hug, B.A., Heusel, J.W. and Ley, T.J. (1996) Long-range disruption of gene expression by a selectable marker cassette. *Proc. Natl. Acad. Sci. U S A*, **93**, 13090–13095.
29. Holzenberger, M., Lenzner, C., Leneuve, P., Zaoui, R., Hamard, G., Vaulont, S. and Bouc, Y.L. (2000) Cre-mediated germline mosaicism: a method allowing rapid generation of several alleles of a target gene. *Nucleic Acids Res.*, **28**, e92.
30. Gallardo, T., Shirley, L., John, G.B. and Castrillon, D.H. (2007) Generation of a germ cell-specific mouse transgenic Cre line, Vasa-Cre. *Genesis*, **45**, 413–417.
31. Graham, R.K., Slow, E.J., Deng, Y., Bissada, N., Lu, G., Pearson, J., Shehadeh, J., Leavitt, B.R., Raymond, L.A. and Hayden, M.R. (2006) Levels of mutant huntingtin influence the phenotypic severity of Huntington disease in YAC128 mouse models. *Neurobiol. Dis.*, **21**, 444–455.
32. Strong, M.K., Southwell, A.L., Yonan, J.M., Hayden, M.R., MacGregor, G.R., Thompson, L.M. and Steward, O. (2012) Age-Dependent Resistance to Excitotoxicity in Htt CAG140 Mice and the Effect of Strain Background. *J. Huntingtons Dis.*, **1**, 221–241.
33. Ghosh, R. and Tabrizi, S. (2013) Clinical Aspects of Huntington's Disease. In *Current Topics in Behavioral Neuroscience*. Springer Berlin Heidelberg, pp. 1–29.
34. Heng, M.Y., Detloff, P.J. and Albin, R.L. (2008) Rodent genetic models of Huntington disease. *Neurobiol. Dis.*, **32**, 1–9.
35. Southwell, A.L., Warby, S.C., Carroll, J.B., Doty, C.N., Skotte, N.H., Zhang, W., Villanueva, E.B., Kovalik, V., Xie, Y., Pouladi, M.A., *et al.* (2013) A fully humanized transgenic mouse model of Huntington disease. *Hum. Mol. Genet.*, **22**, 18–34.
36. Van Raamsdonk, J.M., Murphy, Z., Selva, D.M., Hamidizadeh, R., Pearson, J., Petersen, A., Bjorkqvist, M., Muir, C., Mackenzie, I.R., Hammond, G.L., *et al.* (2007) Testicular degeneration in Huntington disease. *Neurobiol. Dis.*, **26**, 512–520.
37. Papalexi, E., Persson, A., Björkqvist, M., Petersén, Å., Woodman, B., Bates, G.P., Sundler, F., Mulder, H., Brundin, P. and Popovic, N. (2005) Reduction of GnRH and infertility in the R6/2 mouse model of Huntington's disease. *Eur. J. Neurosci.*, **22**, 1541–1546.
38. Leavitt, B.R., Guttman, J.A., Hodgson, J.G., Kimel, G.H., Singaraja, R., Vogl, A.W. and Hayden, M.R. (2001) Wild-Type Huntingtin Reduces the Cellular Toxicity of Mutant Huntingtin In Vivo. *Am. J. Hum. Genet.*, **68**, 313.
39. The Huntington Study Group (1996) Unified Huntington's disease rating scale: Reliability and consistency. *Mov. Disord.*, **11**, 136–142.
40. Pouladi, M.A., Graham, R.K., Karasinska, J.M., Xie, Y., Santos, R.D., Petersen, A. and Hayden, M.R. (2009) Prevention of depressive behaviour in the YAC128 mouse model of Huntington disease by mutation at residue 586 of huntingtin. *Brain*, **132**, 919–932.
41. Novak, M.J.U. and Tabrizi, S.J. (2010) Huntington's disease. *BMJ*, **340**, c3109.
42. Van Raamsdonk, J.M., Pearson, J., Slow, E.J., Hossain, S.M., Leavitt, B.R. and Hayden, M.R. (2005) Cognitive dysfunction precedes neuropathology and motor abnormalities in the YAC128 mouse model of Huntington's disease. *J. Neurosci.*, **25**, 4169–4180.
43. Vonsattel, J. (2008) Huntington disease models and human neuropathology: similarities and differences. *Acta Neuropathol.*, **115**, 55–69.
44. Tabrizi, S.J., Scahill, R.I., Owen, G., Durr, A., Leavitt, B.R., Roos, R.A., Borowsky, B., Landwehrmeyer, B., Frost, C., Johnson, H., *et al.* (2013) Predictors of phenotypic progression and disease onset in premanifest and early-stage Huntington's disease in the TRACK-HD study: analysis of 36-month observational data. *Lancet Neurol.*, **12**, 637–649.
45. Gutekunst, C.A., Li, S.H., Yi, H., Mulroy, J.S., Kuemmerle, S., Jones, R., Rye, D., Ferrante, R.J., Hersch, S.M. and Li, X.J. (1999) Nuclear and Neuropil Aggregates in Huntington's Disease: Relationship to Neuropathology. *J.Neurosci.*, **19**, 2522–2534.
46. Wang, C.E., Zhou, H., McGuire, J.R., Cerullo, V., Lee, B., Li, S.H. and Li, X.J. (2008) Suppression of neuropil aggregates and neurological symptoms by an intracellular antibody implicates the cytoplasmic toxicity of mutant huntingtin. *J. Cell Biol.*, **181**, 803–816.
47. Hodges, A., Strand, A.D., Aragaki, A.K., Kuhn, A., Sengstag, T., Hughes, G., Elliston, L.A., Hartog, C., Goldstein, D.R., Thu, D., *et al.* (2006) Regional and cellular gene expression changes in human Huntington's disease brain. *Hum. Mol. Genet.*, **15**, 965–977.
48. Nisenbaum, E.S. and Wilson, C.J. (1995) Potassium currents responsible for inward and outward rectification in rat neostriatal spiny projection neurons. *J. Neurosci.*, **15**, 4449–4463.
49. Klapstein, G.J., Fisher, R.S., Zanjani, H., Cepeda, C., Jokel, E.S., Chesselet, M.F. and Levine, M.S. (2001) Electrophysiological and Morphological Changes in Striatal Spiny Neurons in R6/2 Huntington's Disease Transgenic Mice. *J. Neurophysiol.*, **86**, 2667–2677.
50. Chiu, C.S., Brickley, S., Jensen, K., Southwell, A., McKinney, S., Cull-Candy, S., Mody, I. and Lester, H.A. (2005) GABA Transporter Deficiency Causes Tremor, Ataxia, Nervousness, and Increased GABA-Induced Tonic Conductance in Cerebellum. *J. Neurosci.*, **25**, 3234–3245.
51. Auerbach, W., Hurlbert, M.S., Hilditch-Maguire, P., Wadghiri, Y.Z., Wheeler, V.C., Cohen, S.I., Joyner, A.L., MacDonald, M.E. and Turnbull, D.H. (2001) The HD mutation causes progressive lethal neurological disease in mice expressing reduced levels of huntingtin. *Hum. Mol. Genet.*, **10**, 2515–2523.
52. Harigaya, Y. and Parker, R. (2010) No-go decay: a quality control mechanism for RNA in translation. *Wiley Interdisciplinary Reviews - RNA*, **1**, 132–141.
53. Mattis, V.B., Tom, C., Akimov, S., Saeedian, J., Oestergaard, M.E., Southwell, A.L., Doty, C.N., Ornelas, L., Sahabian, A., Lenaeus, L., *et al.* (2015) HD iPSC-derived neural progenitors accumulate in culture and are susceptible to BDNF withdrawal due to glutamate toxicity. *Hum. Mol. Genet.*, **24**, 3257–3271.
54. The HD iPsc Consortium(2012) Induced Pluripotent Stem Cells from Patients with Huntington's Disease Show CAG-Repeat-Expansion-Associated Phenotypes. *Cell Stem Cell*, **11**, 264–278.

55. Aronin, N., Chase, K., Young, C., Sapp, E., Schwarz, C., Matta, N., Kornreich, R., Landwehrmeyer, B., Bird, E., Beal, M.F., *et al.* (1995) CAG expansion affects the expression of mutant huntingtin in the Huntington's disease brain. *Neuron*, **15**, 1193–1201.
56. Evers, M.M., Schut, M.H., Pepers, B.A., Atalar, M., van Belzen, M.J., Faull, R.L.M., Roos, R.A.C. and van Roon-Mom, W.M.C. (2015) Making (anti-) sense out of huntingtin levels in Huntington disease. *Mol. Neurodegener.*, **10**, 1–11.
57. Liu, W., Chaurette, J., Pfister, E.L., Kennington, L.A., Chase, K.O., Bullock, J., Vonsattel, J.P.G., Faull, R.L.M., Macdonald, D., DiFiglia, M., *et al.* (2014) Increased Steady-State Mutant Huntingtin mRNA in Huntington's Disease Brain. *J. Huntington's Dis.*, **2**, 491–500.
58. Schauwecker, P.E. and Steward, O. (1997) Genetic determinants of susceptibility to excitotoxic cell death: Implications for gene targeting approaches. *Proc. Natl Acad. Sci. USA*, **94**, 4103–4108.
59. Zuccato, C., Valenza, M. and Cattaneo, E. (2010) Molecular Mechanisms and Potential Therapeutical Targets in Huntington's Disease. *Physiol. Rev.*, **90**, 905–981.
60. Markianos, M., Panas, M., Kalfakis, N. and Vassilopoulos, D. (2005) Plasma testosterone in male patients with Huntington's disease: Relations to severity of illness and dementia. *Ann. Neurol.*, **57**, 520–525.
61. Vonsattel, J.P. and DiFiglia, M. (1998) Huntington Disease. *J. Neuropathol. Exp. Neurol.*, **57**, 369–384.
62. Carroll, J.B., Lerch, J.P., Franciosi, S., Spreeuw, A., Bissada, N., Henkelman, R.M. and Hayden, M.R. (2011) Natural history of disease in the YAC128 mouse reveals a discrete signature of pathology in Huntington disease. *Neurobiol. Dis.*, **43**, 257–265.
63. Hedreen, J.C., Peyser, C.E., Folstein, S.E. and Ross, C.A. (1991) Neuronal loss in layers V and VI of cerebral cortex in Huntington's disease. *Neurosci. Lett.*, **133**, 257–261.
64. Kuhn, A., Goldstein, D.R., Hodges, A., Strand, A.D., Sengstag, T., Kooperberg, C., Becanovic, K., Pouladi, M.A., Sathasivam, K., Cha, J.H.J., *et al.* (2007) Mutant huntingtin's effects on striatal gene expression in mice recapitulate changes observed in human Huntington's disease brain and do not differ with mutant huntingtin length or wild-type huntingtin dosage. *Hum. Mol. Genet.*, **16**, 1845–1861.
65. Squitieri, F., Gellera, C., Cannella, M., Mariotti, C., Cislaghi, G., Rubinsztein, D.C., Almqvist, E.W., Turner, D., Bachoud-Levi, A.C., Simpson, S.A., *et al.* (2003) Homozygosity for CAG mutation in Huntington disease is associated with a more severe clinical course. *Brain*, **126**, 946–955.
66. Taketo, M., Schroeder, A., Mobraaten, L., Gunning, K., Hanten, G., Fox, R., Roderick, T., Stewart, C., Lilly, F. and Hansen, C. (1991) FVB/N: an inbred mouse strain preferable for transgenic analyses. *Proc. Natl. Acad. Sci. U S A*, **88**, 2065.
67. Romberg, C., Horner, A.E., Bussey, T.J. and Saksida, L.M. (2013) A touch screen-automated cognitive test battery reveals impaired attention, memory abnormalities, and increased response inhibition in the TgCRND8 mouse model of Alzheimer's disease. *Neurobiol. Aging*, **34**, 731–744.
68. Trueman, R.C., Brooks, S.P., Jones, L. and Dunnett, S.B. (2007) The operant serial implicit learning task reveals early onset motor learning deficits in the Hdh knock-in mouse model of Huntington's disease. *Eur. J. Neurosci.*, **25**, 551–558.
69. Pinto, R.M., Dragileva, E., Kirby, A., Lloret, A., Lopez, E., St. Claire, J., Panigrahi, G.B., Hou, C., Holloway, K., Gillis, T., *et al.* (2013) Mismatch Repair Genes Mlh1 and Mlh3 Modify CAG Instability in Huntington's Disease Mice: Genome-Wide and Candidate Approaches. *PLoS Genet.*, **9**, e1003930.
70. Carroll, J., Southwell, A., Graham, R., Lerch, J., Ehrnhoefer, D., Cao, L.P., Zhang, W.N., Deng, Y., Bissada, N., Henkelman, R., *et al.* (2011) Mice lacking caspase-2 are protected from behavioral changes, but not pathology, in the YAC128 model of Huntington disease. *Mol. Neurodegener.*, **6**, 59.
71. Smith, G.A., Rocha, E.M., McLean, J.R., Hayes, M.A., Izen, S.C., Isacson, O. and Hallett, P.J. (2014) Progressive axonal transport and synaptic protein changes correlate with behavioral and neuropathological abnormalities in the heterozygous Q175 KI mouse model of Huntington's disease. *Hum. Mol.Genet.*, **23**, 4510–4527.
72. Indersmitten, T., Tran, C.H., Cepeda, C. and Levine, M.S. (2015) Altered excitatory and inhibitory inputs to striatal medium-sized spiny neurons and cortical pyramidal neurons in the Q175 mouse model of Huntington's disease. *J. Neurophysiol.*, **113**, 2953–2966.